Late Triassic initial closure of the Mongol-Okhotsk Ocean in the western segment: constraints from sedimentological, detrital zircon ages and paleomagnetic evidence

Pan Zhao, Zhenhua Jia, Bei Xu, Yan Xu, Turbold Sukhbaatar, Erwin Appel, Yan Chen

Journal Pre-proofs

Late Triassic initial closure of the Mongol-Okhotsk Ocean in the western segment: constraints from sedimentological, detrital zircon ages and paleomagnetic evidence

Pan Zhao, Zhenhua Jia, Bei Xu, Yan Xu, Turbold Sukhbaatar, Erwin Appel, Yan Chen

PII: S1342-937X(23)00221-6
DOI: https://doi.org/10.1016/j.gr.2023.08.007
Reference: GR 3110

To appear in: *Gondwana Research*

Received Date: 11 April 2023
Revised Date: 25 June 2023
Accepted Date: 19 August 2023

Please cite this article as: P. Zhao, Z. Jia, B. Xu, Y. Xu, T. Sukhbaatar, E. Appel, Y. Chen, Late Triassic initial closure of the Mongol-Okhotsk Ocean in the western segment: constraints from sedimentological, detrital zircon ages and paleomagnetic evidence, *Gondwana Research* (2023), doi: https://doi.org/10.1016/j.gr.2023.08.007

Late Triassic initial closure of the Mongol-Okhotsk Ocean in the western segment: constraints from sedimentological, detrital zircon ages and paleomagnetic evidence

Pan Zhao[1]*, Zhenhua Jia[1,2], Bei Xu[3], Yan Xu[4], Turbold Sukhbaatar[5,6], Erwin Appel[7], Yan Chen[8]

[1] State Key Laboratory of Lithospheric Evolution, Institute of Geology and Geophysics, Chinese Academy of Sciences, Beijing 100029, China

[2] College of Earth and Planetary Sciences, University of Chinese Academy of Sciences, Beijing 100049, China

[3] Hebei Key Laboratory of Strategic Critical Mineral Resources, Hebei GEO University, Shijiazhuang 050031, China

[4] Ministry of Education Key Laboratory of Orogenic Belts and Crustal Evolution, School of Earth and Space Sciences, Peking University, Beijing, China

[5] Institute of Petrology and Structural Geology, Charles University, Prague, Czech Republic

[6] Institute of Geology, Mongolian Academy of Sciences, Labor Union St., Ulaanbaatar, Mongolia

[7] Department of Geosciences, University Tübingen, 72076, Tübingen, Germany

[8] Université d'Orléans, ISTO, CNRS/INSU, UMR 7327, 45071 Orléans, France

*Corresponding author: panzhao@mail.iggcas.ac.cn

Abstract:

The Mesozoic evolution of the Mongol-Okhotsk Ocean (MOO) has significantly affected the configuration of the modern Asian continent. Although a scissor-like closure of the MOO has long been proposed, when and how the MOO closed are still hotly debated, especially the timing of initial closure of the MOO in its western segment, hindering our understanding of both the evolution of the MOO and tectonics of the northern Asian continent. In order to uncover the timing of initial closure of the MOO, we performed a multidisciplinary study in sedimentology, detrital zircon U-Pb dating and paleomagnetic on the Late Triassic clastic strata from the Tarvagatay Block and the Amuria Block (AMB) on the both sides of the Mongol-Okhotsk Suture. The upper Triassic strata on both sides of the suture were dominated by plant fossil-bearing alluvial-fluvial facies sediments, which unconformably overlain pre-Triassic geological units, indicating a terrestrial setting after the closure of the MOO. Detrital zircon U-Pb dating results revealed consistent age distribution patterns for samples from both sides of the suture with a predominant peak at ~253-251 Ma and a secondary peak at ~359-357 Ma, representing two main arc magmatic events during the bidirectional subduction of the MOO in the Late Devonian-Early Carboniferous and Late Permian-Early Triassic. Coeval Late Triassic paleomagnetic poles were obtained from the northern AMB and Tarvagatay Block, revealing a comparable paleolatitude of the AMB (~31-33°) and Tarvagatay Block (~32-34°) in the Late Triassic, arguing for that the western segment of the MOO should have closed at the Late Triassic. The compilation of sedimentology, detrital zircon U-Pb dating, magmatic and paleomagnetic evidence provides integrated

constraints on the Late Triassic initial closure of the MOO in its western segment.

Keywords: Mongol-Okhotsk Ocean; sedimentology; detrital zircon U-Pb ages; Paleomagnetism; Late Triassic initial closure

1. Introduction

Northeast Asia was built by amalgamation of several cratons and blocks with accommodation of the evolutions of the Paleo-Asian Ocean mainly during the Paleozoic and the Mongol-Okhotsk Ocean (MOO) during the Late Paleozoic-Early Mesozoic (Zhao et al., 1990; 1996; Xiao et al., 2003; Li, 2006; Xu et al., 2013a, b; Van der Voo et al., 2015; Wu et al., 2017; Huang et al., 2018). As the last main oceanic basin in northeastern Asia, the evolution of the MOO has strongly affected the configuration of the Asian continent and reformed old orogenic belts. The MOO was an east-facing bay-shaped ocean between the Siberian Craton (SIB) to the north and the North China Craton-Amuria Block (NCC-AMB) to the south (Kravchinsky et al., 2002; Khanchuk et al., 2015). It was considered as either a branch of the Paleo-Asian Ocean (e.g., Ganbat et al., 2021) or a gigantic bay of the Paleo-Pacific Ocean (e.g., Gordienko et al., 2019). Some researchers proposed that the MOO evolved into a restricted ocean during the Mesozoic that was separated from the Paleo-Pacific Ocean by an island arc and a subduction zone to the east (Seton et al., 2012). The closure of the MOO along the Mongol-Okhotsk suture led to the formation of the Mongol-Okhotsk orogenic belt that extends over 3000 km from the Hangay-Hentey Mountains in central Mongolia,

through northeastern Mongolia and the Amur River region to the Uda bay of the Okhotsk Sea (Fig. 1; Zonenshain et al., 1990; Zorin, 1999). This orogenic belt displays an insignificant topography uplift with respect to that as expected from a typical continental collisional orogeny, leading to a proposal of "soft collision" of the SIB and NCC-AMB (e.g., Jolivet et al., 2017).

Moreover, the closure process of the MOO is highly controversial on its both style and timing. Based on progressively eastward younging of sedimentary deposits and magmatic events along the Mongol-Okhotsk suture, a scissor-like closure from the Late Permian-Triassic in the west to the Late Jurassic in the east has been proposed (Zonenshain et al., 1990; Zorin, 1999; Chanchuk et al., 2015; Wang et al., 2015; Sorokin et al., 2020; Arzhannikova et al., 2020; 2022; Wang et al., 2022). The scissor-like closure is also supported by paleomagnetic relative rotation between the SIB and NCC-AMB during the Triassic to Jurassic (Zhao et al., 1996; Kravchinsky et al., 2002; Cogné et al., 2005; Metelkin et al., 2010; Yi and Meert, 2020). The other models argued for a late Jurassic-earliest Cretaceous simultaneous closure of the MOO based on compilation of paleomagnetic data (Enkin et al., 1992; Van der Voo et al., 2015). In this model, the relative rotation of the SIB with respect to the NCC-AMB only caused a narrowing of the MOO, especially for its eastern segment, and the MOO became a narrow ocean after the Triassic-Jurassic rotation, followed by a simultaneous closure from the west to east (Van der Voo et al., 2015). The key to solve this controversy is to constrain initial closure of the MOO in its western segment. Concerning the timing of the initial closure, previous sedimentary and magmatic studies supported a Late

Triassic-Early Jurassic closure (Zonenshain et al., 1990; Donskaya et al., 2013), whereas paleomagnetic data indicate either a Permian-Triassic or a Late Jurassic initial closure in the western segment (Zhao et al., 1996; Van der Voo et al., 2015). This temporal discrepancy severely hinders our understanding of the evolution of the MOO.

Therefore, in this study we integrate sedimentological investigation, detrital zircon dating as well as paleomagnetic measurement from both sides of the Mongol-Okhotsk suture in its western segment, with compilation of other geological evidence to constrain the initial closure of the MOO, and further discuss the evolution of the MOO.

2. Geological framework the Mongol-Okhotsk suture and surrounding blocks

2.1 The SIB and accreted blocks in the north of the suture

The SIB is a stable craton with a basement made of Archean blocks and Paleoproterozoic foldbelts (Rosen, 2003; Glebovitsky et al., 2008). Amalgamation of several Archean blocks in the age of 2.1-1.8 Ga resulted in the cratonization of the SIB (Rosen et al., 1994; Gladkochub et al., 2006; Glebovitsky et al., 2008). During the late Mesoproterozoic-Neoproterozoic, several blocks were situated within the Paleo-Asian Ocean near the margin of the SIB, including the Khamar Daban, Tuva-Mongolia, Barguzin, Kansk-Derba, Tarvagatay Blocks (Gusev and Khain, 1996). The accretion of these blocks to south the margin of the SIB started at the Neoproterozoic and lasted until the Early Paleozoic (Jolivet et al., 2009). For example, the Barguzin block collided with the SIB during the Late Neoproterozoic-Early Cambrian, evidenced by 600-550 Ma metamorphic and magmatic events within the Baikal-Muya ophiolite belt and coeval thick molasses sediments (Delvaux et al., 1995; Gusev and Khain, 1996). The

Tuva-Mongolia block accreted to the south margin of the SIB in the Cambrian represented by a regional metamorphism at 530-485 Ma (Fedorovskii et al., 1993), which was supported by paleomagnetic studies (Kravchinsky et al., 2001). These Neoproterozoic-Cambrian accreted blocks constituted the new southern margin of the SIB that faced to the northern side of the MOO in its western segment (Fig. 1). Therefore, the closure of the MOO in its western segment could be actually caused by the collision between the AMB and these accreted blocks.

Two episodes of continental arc magmatism from the Silurian to Permian-emplaced along the southern margin of the accreted block (the Tarvagatay Block) due to the northward subduction of the MOO (Fig. 2). The Silurian-early Carboniferous period recorded the first episode of this arc magmatism, represented by volcanic and intrusive rocks with arc-like affinity (Fig. 2; Zonenshain et al., 1990; Donskaya et al., 2013; Gordienko et al., 2019; Ling et al., 2021). The most intensive magmatic pulse for this episode occurred at the late Devonian-early Carboniferous, revealed by the late Devonian age peaks in detrital zircon distribution patterns (Bussien et al., 2011). Thereafter, a magmatic quiescence period occurred until to the Permian re-initiation of arc magmatism that reworked ubiquitous Silurian-early Carboniferous magmatic rocks (Fig. 2; Bussien et al., 2011; Sun et al., 2013; Wang et al., 2022). Silurian-Permian marine strata deposited along the southern margin of the Tarvagatay Block (Zonenshain et al., 1990; Bussien et al., 2011), representing the fore-arc basin sedimentation in the active convergence boundary due to the northward subduction of the MOO, which were unconformably overlain by the Late Triassic conglomerate and late Triassic-early

Jurassic intracontinental volcanic rocks (Fig. 2; Badarch et al., 2002; Bussien et al., 2011).

2.2 The AMB in the south of the suture

The AMB is constituted by several Precambrian blocks, such as the Ereendavaa, Erguna, Xing'an, South Gobi, South Mongolia, Songliao blocks from north to south. Welding of these blocks occurred during the Cambrian-Carboniferous accommodating with the evolution of the Paleo-Asian Ocean (Zhou et al., 2018). The Ereendavaa block, named also as the Kerulen block in the new tectonic division of Mongolia (Tomurtogoo, 2014), extends eastward into Russia and northeast China and connects with the Erguna Block (Bardach et al., 2002). The collision between the Erguna block and the Xing'an block along the Xinlin-Xiguitu suture was suggested to occur at ca. 500 Ma (Liu et al., 2017), constrained by ca. 490 Ma blueschist metamorphism (Zhou et al., 2015), ca. 500 Ma high-grade metamorphic rocks of the Xinghuadukou Group (Zhou et al., 2011), and 494-480 Ma post-orogenic A-type granites (Ge et al., 2005). The amalgamation of the Xing'an block with the Songliao Block along the Hegenshan-Heihe suture was thought most likely to happen at the Early/Late Carboniferous boundary (Liu et al., 2017) or at the Late Carboniferous-Early Permian boundary (Fu et al., 2021). The welded AMB collided with the northern margin of the NCC following the closure of the Paleo-Asian Ocean probably in the Late Paleozoic (Xiao et al., 2003; Zhao et al., 2013). The unified NCC-AMB then continued to converge with the SIB during the Mesozoic until to the final closure of the MOO.

Similar to the Tarvagatay Block to the northern side of the Mongol-Okhotsk suture,

two episodes of continental arc magmatism have been identified from the Ereendavaa block on the northern part of the AMB resulted from the southward subduction of the MOO (Fig. 2; Kelty et al., 2008; Bussien et al., 2011; Sun et al., 2013; Xu et al., 2013b; Mao et al., 2021). The first episode of arc magmatism was later than that in the Tarvagatay Block, Devonian-early Carboniferous volcanic and intrusive rocks with arc-like affinity are widely distributed in the Ereendavaa block (Fig. 2; Bussien et al., 2011; Donskaya et al., 2013), with the most intensive magmatic pulse in the early Carboniferous revealed by the detrital zircon distribution pattern (Kelty et al., 2008; Bussien et al., 2011). The late Carboniferous magmatic quiescence period was recorded on the Ereendavaa block until to the Permian-Triassic arc magmatic event (Fig. 2; Bussien et al., 2011; Tang et al., 2014; Zhao et al., 2017; Sheldrick et al., 2020; Mao et al., 2021). Along the northern margin of the Erguna block, Jurassic magmatic rocks have been widely identified, representing the Jurassic southward subduction of the MOO (Sun et al., 2013; Tang et al., 2016; Wang et al., 2022). Silurian-Permian marine strata were deposited along the northern margin of the western AMB (Zonenshain et al., 1990), representing the forearc basin sedimentations in the active convergence boundary due to the southward subduction of the MOO. These Paleozoic strata and intrusive rocks were also unconformably overlain by the Late Triassic conglomerates, which are evolved upward into late Triassic-early Jurassic intracontinental volcanic rocks and early Jurassic fluvial-lacustrine sediments (Fig. 2; Badarch et al., 2002; Bussien et al., 2011).

2.3 The Mongol-Okhotsk suture

The Mongol-Okhotsk suture is a tectonic mélange belt between the SIB and the AMB that represents relic of the MOO. It comprises metasedimentary and metavolcanic rocks, limestones, cherts, ophiolite assemblage with the ages from the Silurian to earliest Triassic (Badarch et al., 2002; Tomurtogoo et al., 2005). One of the striking features of this suture is the thick late Silurian-Devonian pelagic deep-water radiolarian cherts preserved in its western segment around the Hangay-Hentey Mountain regions (Fig. 2; Kashiwagi et al., 2004; Kurihara et al., 2009). Two ophiolite assemblages, namely the Adaatsag ophiolite and the Khuhu Davaa ophiolite, have been identified from central and northeastern Mongolia that are composed of cherts, gabbros, metabasalts and ultramafic rocks, with greenschists and gabbro-amphibolites as matrix (Tomurtogoo et al., 2005; Zhu et al., 2018). Zircon U-Pb dating results revealed their formation in the ages of 325-314 Ma, indicating the Late Carboniferous formation of the oceanic crust (Fig. 2; Tomurtogoo et al., 2005; Zhu et al., 2018). The late Permian to early Triassic fossiliferous marine sediments and cherts within the suture in northeastern Mongolia indicate the existence of the MOO during these periods (Zonenshain et al., 1990).

This suture extends to Russia, represented by the Onon island arc in the Trans-Baikal region, which was produced by the subduction of the MOO (Zorin, 1999). Two episodes of oceanic subduction beneath the Onon island arc were proposed (Zorin, 1999). The first episode from the Devonian to Early Carboniferous caused Devonian-Early Carboniferous volcanic rocks and marine turbidites, which ceased prior to the Late Carboniferous, evidenced by Late Carboniferous-Early Permian clastic marine

deposits on the island shelf (Zorin et al., 1995). Paleomagnetic results suggested that the Onon island arc was distant from both the SIB and AMB in the Late Carboniferous-Early Permian (Kuzmin and Kravchinsky, 1996). The second episode of the subduction initiated at the Late Permian, resulted in the formation of Late Permian to Triassic basaltic andesites, andesites, dacites and marine sediments. Its youngest age reported from the Onon island arc is at ca. 197 Ma, suggested that the subduction of the MOO beneath the Onon arc had lasted at least until the Early Jurassic (Zorin, 1999).

This tectonic mélange belt was firstly considered as an accretionary wedge (Sengör et al., 1993). Under concept of the Mongol-Okhotsk belt, these Paleozoic pelagic deep-water sediments were interpreted as an accretionary wedge in the trench along the southern margin of the SIB (Zorin, 1999). Gordienko (1987; 2006) considered that these rocks represented a back-arc sediments formed by the northward subduction of the MOO. On the contrary, Badarch et al. (2002) proposed that the thick Devonian-Carboniferous pelagic deep-water sediments within this belt represent a coherent turbidite sequence overlying a cratonic basement. Despite these debates, it is now well accepted that this belt represents the final suture of the MOO, marking the collision between the SIB and AMB.

3. Sedimentology and detrital zircon dating

The upper Triassic strata are distributed in central Mongolia on both sides of the Mongol-Okhotsk suture (Figs. 2, 3), unconformably overlying pre-Late Triassic geological units, e.g., the metamorphic basement, Devonian-Permian marine sediments,

and Permian volcanic rocks, representing a regional unconformity (Badarch et al., 2002). The upper Triassic strata are characterized by terrestrial facies coarse-grained sediments including alluvial and fluvial conglomerates and sandstone with abundant plant fossils. We measured five sections for sedimentological investigations and made detrital zircon dating from both sides of the suture. Positions of these five sections are marked in Figure 3.

3.1 Sedimentological studies

To the north of the Mongol-Okhotsk suture, three sections of the upper Triassic strata were investigated near the town of Avdzaga in central Mongolia (Fig. 3a). The upper Triassic strata in this region are conglomerate-dominated with hundreds of meter-thick basal conglomerates (Fig. 4), containing pebbles and cobbles of different rock types, such as chert, greenschist, granite, volcanic rocks, sandstone (Fig. 5a, b). All pebbles and cobbles are badly sorted and poorly rounded (Fig. 5a, b), with a matrix-supported fabric of finer sediments as matrix, indicating rapidly accumulated alluvial fan deposits. In the middle part of the strata, interlayers of conglomerates and sandstone can be observed (e.g., the upper part of Section N-1 and middle part of Section N-2; Figs. 4, 5d, e). It should be noted that pebbles within the conglomeratic layers are well rounded, and cross-beddings and parallel beddings can be observed in the sandstone layers (Fig. 5f, g), indicating fluvial deposition with a strong hydrodynamic condition. Abundant plant fossils have been identified from sandstone layers, e.g., *Tersiella* sp., *Taeniopteris* sp., *Pelourdea* sp., (Fig 5h, i), providing reliable constraints of the depositional age of these upper Triassic strata (Khosbayar et al., 1987). The upper part

of the upper Triassic strata is dominated by sandstone with several conglomerate interlayers (Fig. 4).

To the south of the Mongol-Okhotsk suture, two cross sections were studied near the towns of Adaatsag and Delgerhaan in central Mongolia (Fig. 3b, c). For the upper Triassic strata near Adaatsag, conglomerates are predominant with rounded cobbles of ca. 20 cm in diameter in its basal part (Fig. 6a, b), showing an upward fining sequence (Fig. 4). Cross-beddings and parallel beddings can be observed in the pebble-bearing sandstone and sandstone layers (Fig. 6c), indicating fluvial deposition with a strong hydrodynamic condition. Red sandstone layers with parallel beddings dominate the upper part of section S-1 (Fig. 6d). The section S-2 near Delgerhaan is composed of conglomerate in the lower part, and pebble-bearing sandstone and sandstone in the upper part, showing an upward fining sequence (Fig. 4). The upper Triassic strata from both regions contains abundant plant fossils within sandstone layers (Fig. 6e, f), e.g., *Paracalamites* sp., *Taeniopteris* sp., (Kalimulin et al., 1968; Adya et al., 1970).

3.2 Detrital zircon dating and provenance investigation

Eight sandstone samples (4 from sections to the north and other 4 from sections to the south of the suture; Fig. 4) were collected for detrital zircon U-Pb dating and further provenance investigations.

3.2.1 Analytical methods

Zircon grains were extracted from samples firstly by conventional heavy liquid and magnetic separation technique, and then the remaining grains were hand-picked under a binocular microscope. Hand-picked zircon grains were mounted in epoxy and then

polished to half to expose zircon interiors. Optical photographs under both reflected and transmission light and cathodoluminescence (CL) imaging were performed to show internal texture of zircon grains for selecting optimal positions for dating. Zircon U-Pb dating were conducted with LA-ICP-MS at the Hebei Key Laboratory of Strategic Critical Mineral Resources (Hebei GEO University) using a LA-ICP-MS system with a 193-nm ArF Excimer laser (RESOlution-LR) and a quadrupole ICP-MS (THERMO-ICAP RQ). Laser spot size was set to 29 μm for all analyses, laser energy density at 3 J/cm^2 and repetition rate at 8 Hz. The procedure of laser sampling 10 seconds blank, 40 seconds sampling ablation, and 20 seconds sample-chamber flushing after the ablation. NIST 610 glass and Si were used as external and internal standards for calibrations of zircon analyses. U–Pb isotope fractionation effects were corrected using zircon 91500 as external standard, with zircon standard GJ_1 and Plešovice as secondary standard to supervise the deviation of age measurement/calculation. Element concentrations and isotopic ratios were calculated with Iolite v. 3.1 (Paton, 2010). For common lead correction, we followed Andersen's (2002) method. Concordia ages were calculated by Isoplot/Excel (3.0), with the weighted mean ages at 95% confidence level (Ludwig, 2003). For each sample, 90 zircon grains were analyzed and analytical results with disconcordance larger than 10% were excluded for further discussion.

3.2.2 Detrital zircon dating results

For sandstone samples from the north of the suture (Fig. 3), zircon grains are euhedral to subhedral, ranging from 40-100 μm in width and 80-200 μm in length with well-developed oscillatory growth zoning (Fig. 7). The Th/U ratios range from 0.13 to

2.04, indicating magmatic origin. Totally, 357 out of 360 dated zircon grains give concordant ages (Supplementary Table 1). Only 5 of all concordant ages are over 1.0 Ga (Supplementary Table 1), furthermore, as the number of this age is too small to give statistical meaningful information, it is excluded for the provenance investigation. Age data from the four samples give consistent distribution patterns with two peaks at ~254 Ma and ~350 Ma, with few Neoproterozoic grains (Fig. 8a-d). The only difference is that for samples # M17-23 and M18-01 from Section N1, the peak at ~350 Ma is predominant, whereas the peak at ~254 Ma is dominant for samples # M17-26 and M18-02 from Sections N2 and N3 (Fig. 8a-d). This difference can be ascribed to provenance change with gradual erosion and deposition. Put all ages from these four samples together, a bimodal-peak pattern can be presented with main peaks at 253 and 359 Ma-(Fig. 9a).

Zircon grains of samples from the south of the suture are euhedral to subhedral, ranging from 40-70 μm in width and 50-120 μm in length with well-developed oscillatory growth zoning (Fig. 7). The Th/U ratios range from 0.19 to 3.64, indicating magmatic origin. Totally, 340 out of 360 dated zircon grains give concordant ages with 4 grains giving ages over 1.0 Ga (Supplementary Table 1), which are too few for provenance analysis. Sample #M18-04 from the bottom of Section S1 shows a similar age distribution pattern with those of samples in the north of the suture (Fig. 8h). The other three samples show a consistent single peak at ~253-251 Ma (Fig. 8e-g). All age data from these four samples constituted a single-peak pattern with a predominant peak at 251 Ma and small peak at 357 Ma (Fig. 9c).

4. Paleomagnetic constraints

From the paleomagnetic aspect of view, the best way to constrain timing of continental collision is to compare coeval paleomagnetic data of blocks from both sides of the suture (Van der Voo et al., 2015). Therefore, we collected paleomagnetic samples from the upper Triassic strata from both sides of the suture, with 12 sites from Section S-1 and S-2 in the south and 11 sites from Section N-1 and N-2 in the north of the suture (Table 1; Fig. 4). Results of samples from Sections N-1 and N-2 have been published (Zhao et al., 2023) and will be used for comparison here.

4.1 Analytical methods

Core samples were cut into standard cylinder specimens with length of 2.2 cm. Rock magnetic experiments were firstly performed to identify magnetic carriers. High-temperature magnetic susceptibility (κ-T curves) were measured using a CS3 furnace coupled MFK-1 Kappabridge. Magnetic hysteresis loops were measured using a MicroMag 2900 Alternating Gradient Magnetometer, and acquisition of IRM were made with a Minispin spinner magnetometer after imparting IRMs with a MMPM9 pulse magnetizer. Rock magnetic investigations were performed in the Paleomagnetism Laboratory of University of Tübingen.

Standard specimens were subjected to stepwise demagnetization. Thermal demagnetization was progressively applied to most specimens to remove magnetic remanences by 15-17 steps up to 685˚C, with temperature intervals of 20˚C to 100˚C. For yellow sandstone from Section S-2, alternating magnetic field technique was also

used for comparison with thermal demagnetization. For each site, 6-8 specimens were demagnetized. We used a TD-48SC thermal demagnetizer for demagnetization, and after each step magnetic remanence measurements were carried out with a 2G pulsetube DC-SQUID magnetometer at University of Tübingen.

Principal component analysis (Kirschvink, 1980) was used for separation of magnetic remanence directions, and mean directions were computed by Fisher statistics (Fisher, 1953). The paleomagnetic software packages of PaleoMac (Cogné, 2003) and Remasoft (designed by AGICO) were used for data analysis.

4.2 Rock magnetic results

For red sandstone samples from Section S-1, thermomagnetic (κ-T) curves show irreversible heating and cooling behaviors (Fig. 10a). The heating curve shows a significant decrease of the magnetic susceptibility at 580 °C, followed by a gradual decrease until 700 °C (Fig. 10a). IRM acquisition curve shows a rapid increase of magnetization before 200 mT and a gradual increase without saturation at 2 T (Fig. 10b). Both κ-T and IRM acquisition curves indicate the coexistence of magnetite and hematite as main magmatic carriers, supported by the hysteresis loop that yields a coercivity (Bc) value of ~15.4 mT and Mr/Ms ratio at ~0.24 (Fig. 10c). For yellow sandstone from Section S-2, the heating curve shows a gradual decrease of the magnetic susceptibility values without clear drop (Fig. 10d). The IRM acquisition curve shows a rapid increase of magnetization up to 90% saturation before 200 mT (Fig. 10e) and the hysteresis loop shows a coercivity (Bc) value of ~4.4 mT and Mr/Ms ratio at ~0.03 (Fig. 10f), both of which indicate a predominant magnetite as the main magnetic carrier.

4.3 Paleomagnetic directional analysis

Specimens from Section S-1 display single magnetic component (Fig. 11), which can be considered as the characteristic remanent magnetization (ChRM). The ChRM directions show antipodal normal and reversed polarities (Fig. 11). With 27 specimens, a mean direction was calculated at D_g/I_g = 248.2˚/-53.2˚ (k_g = 13.4, α_{95g} = 7.9˚) in geographic coordinates and D_s/I_s = 32.6˚/-39.1˚ (k_s = 13.4, α_{95s} = 7.9˚) after tilt-corrections (Table 1; Fig. 12a, b). The reversal test of MaFadden and McElhinny (1990) is positive at level-C, indicating that the ChRM should be primary acquired during deposition.

Most specimens from Section S-2 show single component and only normal polarity was observed (Fig. 11), which we considered as the ChRM. A mean direction was calculated at D_g/I_g = 309.7˚/71.3˚ (k_g = 9.5, α_{95g} = 9.5˚) in geographic coordinates and D_s/I_s = 318.9˚/36.9˚ (k_s = 9.5, α_{95s} = 9.5˚) after tilt-corrections with 27 specimens (Table 1; Fig. 12a, b). Although neither fold test nor reversal test is available, this magnetic direction in stratigraphic coordinates is different from post-Triassic ones of the NCC-AMB (Wu et al., 2017; Huang et al., 2018), which may argue for its primary nature.

Before calculating the corresponding corresponding virtual geomagnetic poles (VGP) of these two mean directions, the inclination shallowing needs to be adjusted. A typical flattening factor f = 0.6 has been applied to paleomagnetic data in tectonic studies of eastern Asia (Van der Voo et al., 2015; Wu et al., 2017), which is further supported by the case study from Triassic sedimentary rocks in the northern NCC (Zhou et al., 2017). Therefore, for a better comparison with previously reported paleomagnetic

data, we apply this flattening factor (f = 0.6) to our newly acquired Triassic data and re-calculated the mean direction of D_s/I_s = 32.6˚/-53.7˚ (k_s = 13.4, α_{95s} = 7.9˚) for Section S-1, and D_s/I_s = 318.9˚/51.4˚ (k_s = 9.5, α_{95s} = 9.5˚) for Section S-2 in stratigraphic coordinates (Table 1). The corresponding VPGs were therefore calculated at λ/φ = -4.1˚N/80.3˚E (A_{95} = 9.2˚) with a paleolatitude of 34.2° ± 9.2° for Section S-1, and λ/φ = 55.4˚N/18.6˚E (A_{95} = 10.6˚) with a paleolatitude of 32.1° ± 10.6° for Section S-2 (Table 1; Fig. 12). We plot these two newly obtained poles and reported Late Triassic poles from the AMB, Tarvagatay Block and SIB in a stereoplot, together with APWPs of the NCC and SIB for comparison (Fig. 13). The five poles from the AMB and Tarvagatay Block aligned along a small circle centered on the sampling location, indicating similar paleolatitude of the AMB and the Tarvagatay Block at the Late Triassic.

5. Discussion

5.1 Late Triassic initial closure of the MOO in its western segment

5.1.1 Geological perspective

The timing of the initial closure of the MOO in its western segment is poorly constrained due to limited geological records and paucity of studies. Zonenshain et al. (1990) proposed a change of geodynamic condition during 260-230 Ma in the western AMB, where the activity of the East Mongolia volcanic belt ceased, replaced by quiet subsidence and clastic sedimentation in a continental and near-shore environment. This geodynamic transition might be related to the cessation of the subduction of the MOO beneath the AMB. From sedimentary comparison, an Early-Middle Triassic

sedimentary hiatus was observed from the Tarvagatay and Bayangol Blocks on the northern side, and the Baydarg, Ereendavaa, and Herlen blocks on the southern side of the Mongol-Okhotsk suture in central and eastern Mongolia, with the Late Triassic molasses overlying on the pre-Triassic geological units, indicating a Triassic regional unconformity (Fig. 2; Badarch et al., 2002). This regional unconformity may suggest that the western segment of the MOO have closed at the Middle-Late Triassic. In this study, we identified similar plant fossil-bearing alluvial-fluvial facies sediments from coeval upper Triassic strata on both sides of the Mongol-Okhotsk suture, which unconformably covered the metamorphic basement, Devonian-Carboniferous marine sediments and Permian volcanic rocks (Fig. 14). Based on these sedimentary characteristics, a non-marine geological setting after the closure of the MOO can be reasonably proposed for the Late Triassic clastic sediments on both sides of the suture. Furthermore, sedimentological investigations and detrital zircon dating on the Mesozoic strata in the western Transbaikalia have showed that the Khangay and Khentey regions were dominated by terrestrial deposits at least since the earliest Jurassic, indicating a wide uplifted plateau formed due to closure of the Mongol–Okhotsk Ocean in its western segment (Arzhannikova et al., 2020).

Our detrital zircon U-Pb dating results show similar age distribution patterns for samples from both sides of the suture with a predominant peak at ~253-251 Ma and secondary peak at ~359-357 Ma (Fig. 9a, c), indicating a similar provenance for the upper Triassic strata. The earliest Carboniferous arc magmatism along the southern margin of the Mongol-Okhotsk suture has been revealed by detail zircon studies from

Carboniferous strata (Fig. 9d; Kelty et al., 2008). However, as their samples are from the northern part of the Mongol-Okhotsk suture and display no early Carboniferous detrital zircons, the northward subduction of the MOO in the early Carboniferous can be questioned although the authors also noticed that there are Devonian-Carboniferous magmatic rocks distributed in the north of the Mongol-Okhotsk suture (Kelty et al., 2008). However, this can be ascribed to that only Cambrian-Silurian deposits have been probably sampled for this purpose, therefore, it is impossible to obtain early Carboniferous detrital zircons. On the contrary, the two Carboniferous samples (# 3 and 4) from the northern margin of the suture indeed display predominant early Carboniferous peaks, similar as samples from the south (Fig. 9b; Kelty et al., 2008). Although the authors considered that they were deposited in a similar tectonic setting as samples from the south and displaced in the northern margin of the Mongol-Okhotsk suture due to a northeast-striking and right-lateral strike-slip faulting or a large north-dipping thrusting, it is more reasonable to consider that they were derived directly from nearby Devonian-Carboniferous magmatic rocks in the northern of the Mongol-Okhotsk suture as there is no clear evidence of this kind of fault or thrust. This new interpretation is supported by further detrital zircon dating results from Permian-Jurassic strata in the north of the Mongol-Okhotsk suture, which revealed abundant Early Carboniferous detrital zircon ages (Bussien et al., 2011). Therefore, the ~359-357 Ma peak was contributed by Devonian-Carboniferous arc magmatic rocks along both sides of the Mongol-Okhotsk suture. The predominant ~253-251 Ma peak is mainly from the Selenge and Middle Gobi Permian-Triassic volcanic-plutonic belts along the

Mongol-Okhotsk suture (Badarch et al., 2002). These two belts were interpreted as either continental rift zones (Kovalenko and Yarmolyuk, 1990) or the Andean type continental margin of the MOO (Zorin, 1999; Parfenov et al., 1999).

Meanwhile, the Late Triassic alkaline magmatism observed in the Hangay-Hentey region indicate an extensional setting for their emplacement, suggesting a Late Triassic closure of the MOO in its western segment (Donskaya et al., 2013). Recently, a compilation of magmatic rocks along the Mongol-Okhotsk Suture revealed that Late Triassic alkaline granitic plutons intruded into the Mongol-Okhotsk suture (Wang et al., 2022). These Late Triassic granitic plutons in the age of 220–210 Ma mainly consist of A2-type high-K calc-alkaline, biotite and hornblende-biotite granites that intruded into folded and foliated accretionary complexes and ophiolitic mélange of the suture, and they can be considered as stitching plutons, therefore, suggesting that the MOO should have closed in the western segment at least by ca. 210 Ma (Fig. 14; Wang et al., 2022).

5.1.2 Paleomagnetic perspective

As the initial closure of the MOO was resulted from collision between the northwestern AMB and Tarvagatay Block in the southwestern SIB, a comparison of paleomagentic data from these two parts will be the best way to constrain its closure. However, paleomagnetic data in these two parts are scarce, hindering our precise estimation of the MOO's initial closure in its western segment. In fact, Pruner (1992) reported a preliminary paleomagnetic pole from the Late Triassic volcanic rocks in the Tarvagatay Block, revealing a low paleolatitude of ~32.8° ± 16.8°N (Table 2). However,

as the big uncertainty of this result, its tectonic significance has not been well acknowledged. Recently, we reported a new Late Triassic pole from the Tarvagatay Block, which gave a paleolatitude of 31.1° ± 9.0° N (Table 2; Fig. 13; Zhao et al., 2023), consistent with that obtained by Pruner (1992). These two independent studies constrain a relative low paleolatitude for the Tarvagatay Block during the Late Triassic. In this study we obtained two poles from the northwestern part of the AMB with consistent paleolatitudes of 34.2° ± 9.2°N and 32.1° ± 10.6°N (Table 2), and the two poles are aligned on one small circle that transects two poles from the Tarvagatay Block (Fig. 13), indicating the consistent paleolatitude of the AMB and Tarvagatay Block in the Late Triassic (Table 2; Fig. 14). Therefore, the AMB should have collided with the Tarvagatay Block during the Late Triassic, suggesting that the western segment of the MOO should have been closed by the Late Triassic.

In conclusion, multidisciplinary evidence from sedimentology, detrital zircon dating, magmatism and paleomagnetism argue for that the western segment of the MOO should have been closed at the Late Triassic (Fig. 14). Our study solves the previous contradiction between geological and paleomagnetic results, therefore, provides integrated constraints on the Late Triassic initial closure of the MOO.

5.2 Eastward progressive closure of the MOO

It has long been accepted that the MOO was an east-facing bay-shaped ocean in the Late Paleozoic. Based on limited paleomagnetic data, Zonenshain et al. (1990) suggested that in the Early Permian, after the western end of the AMB welding with the southeastern margin of the SIB in the Hangay-Hentey region, the two continental

margins displayed a ca. 130° intersection angle. This estimate is supported by following paleomagnetic studies that constrained a meridional alignment of the south margin of the SIB and northeast facing of the north margin of the AMB (Kravchinsky et al., 2002; Zhao et al., 2020). Since then, a clockwise rotation of the SIB and counterclockwise rotation of the AMB and NCC led to gradual closure of the MOO, which is also supported by geological evidence from sedimentary and magmatic aspects.

The Mongol-Okhotsk suture is surrounded by numerous calc-alkaline magmatic rocks related to bidirectional subductions of the MOO. Two main episodes of magmatism in the age of Devonian-early Carboniferous and Permian-Middle Triassic are nearly symmetrically distributed on both sides of the suture (Sorokin et al., 2005; Kelty et al., 2008; Bussien et al., 2011; Ruppen et al., 2014; Ganbat et al., 2021). Triassic-Jurassic magmatic rocks, on the other hand, show a clear eastward younging trend, with the Early-Middle Triassic magmatic rocks occurring in both the western segment in central Mongolia and the eastern segment in the Amur River region, whereas the Late Triassic-Early Jurassic ones are only distributed in the eastern segment in northeastern Mongolia and the Amur River region (Sorokin et al., 2010; Xu et al., 2013b; Sun et al., 2013; Tang et al., 2014; Ganbat et al., 2021; Ovchinnikov et al., 2023). Meanwhile, sedimentary studies also revealed an eastward progressive transition from marine to nonmarine facies. Continental molasses were first observed from the upper Triassic strata in the Hangay-Hentey region of the westernmost part of the suture (Zonenshain et al., 1990), whereas the transition from marine flysch to nonmarine molasses occurred at the boundary of Early/Middle Jurassic in the eastern

Transbaikal region of the central segment (Demonterova et al., 2017; Jolivet et al., 2017; Arzhannikova et al., 2020). For the Upper Amur-Mohe foreland basin in the eastern segment, this sedimentary transition was also observed in the Middle-Late Jurassic (Li et al., 2004; He et al., 2005; Smirnova et al., 2017; Zaika et al., 2018; Sorokin et al., 2020) or even Latest Jurassic (Yang et al., 2015; Chen et al., 2022). Moreover, detrital zircon dating results reveal the absence of detrital zircons younger than 171 Ma in the sedimentary rocks in the Upper Amur and other basins of the eastern Mongol-Okhotsk belt, implying that the final closure could have taken place at the boundary of the Early and Middle Jurassic (Sorokin et al., 2020). This proposal is consistent with the Early Mesozoic thermal event occurred in this region (Sorokin et al., 2023) and also supported by recently paleomagnetic study. Yi and Meert (2020) integrated geological and paleomagnetic evidence and argued for a Middle Jurassic (~174 Ma) closure of the MOO. The eastward younging trend of both magmatic and sedimentary records led to the proposal of scissor-like closure of the MOO.

However, the scissor-like closure of the MOO was challenged by paleomagnetic investigations. Based on comparison of paleomagnetic poles from the SIB and NCC-AMB, Van der Voo et al. (2015) proposed a progressive narrowing model of the MOO during the Triassic-Jurassic period. In this model, the relative rotation of the SIB with respect to NCC-AMB caused shrinking of the MOO much faster in the east than in the west. However, this process did not lead to an eastward gradual closure of the MOO, nevertheless, it resulted in a nearly identical width of the MOO from west to east in the Late Jurassic and a simultaneous closure of the MOO in the Late Jurassic-Early

Cretaceous (Van der Voo et al., 2015). This progressive narrowing model of the MOO is similar as that proposed by Enkin et al. (1992). But Enkin et al. (1992) emphasized on a northward movement of the NCC-AMB along a sinistral strike-slip fault at its western margin that caused the closure of the MOO. It is worth noting that both two proposed models are contradictory with geological evidence, especially about the initial closure of the MOO in its western segment. This may be caused by lack of reliable Triassic paleomagnetic poles, which presents the key period for the initial closure of the MOO. The new Late Triassic paleomagnetic data obtained in this study suggest similar paleolatitude of the AMB and Tarvagatay Block on both sides of the Mongol-Okhotsk suture, indicating that the western segment of MOO should have been closed at the Late Triassic, consistent with geological evidence. After the initial collision of the MOO in the Hangay-Hentey region, this region can be considered as a pivot, around which SIB and NCC-AMB rotated relatively, leading to a gradually closure of the MOO from west to east in a scissor-like way (Van der Voo et al., 2015; Xu et al., 2013b; Wang et al., 2022).

5. Conclusions

From our new and compiled sedimentological, detrital zircon U-Pb dating, and paleomagnetic data obtained for the upper Triassic strata from both sides of the western segment of the Mongol-Okhotsk suture, we obtain the following conclusions:

(1) Plant fossil-bearing alluvial-fluvial facies sediments were identified from coeval upper Triassic strata on both sides of the western segment of the Mongol-Okhotsk suture, unconformably overlying on the metamorphic basement, Devonian-

Carboniferous marine sediments and Permian volcanic rocks. Based on these sedimentary characteristics, we proposed a non-marine geological setting after the closure of the MOO for the Late Triassic clastic sediments on both sides of the suture. Detrital zircon U-Pb dating results show similar age distribution patterns for samples from both sides of the suture with a predominant peak at ~253-251 Ma and secondary one at ~359-357 Ma, indicating similar provenance for the upper Triassic strata. These two peaks represent two main arc magmatic events during bidirectional subductions of the MOO in the Late Devonian-Early Carboniferous and Late Permian-Early Triassic.

(2) Coeval Late Triassic paleomagnetic poles obtained from the northern AMB and Tarvagatay Block on both sides of the Mongol-Okhotsk suture revealed consistent paleolatitude of the AMB (~31-33°) and Tarvagatay Block (~32-34°) in the Late Triassic, arguing for that the western segment of the MOO should have been closed at the Late Triassic.

(3) The comparable sedimentological, detrital zircon U-Pb dating, magmatic and paleomagnetic evidence provide integrated constraints on the Late Triassic initial closure of the MOO. After initial closure of the MOO in the Hangay-Hentey region, furthermore, this region can be considered as a pivot, around which the SIB and NCC-AMB rotated relatively, leading to a gradually closure of the MOO from west to east in a scissor-like way.

Declaration of Competing Interest

The authors declare that no known competing financial interests or personal

relationships that could have appeared to influence the work in this paper.

Acknowledgments

This study was funded by the National Natural Science Foundation of China (92155203, 41888101 and 42172248). Yanyang Wang and Yanjie Zhang are acknowledged for help in the fieldtrip. We thank the Associate Editor Joseph Meert for handling this manuscript, and Andrey Sorokin for their constructive comments that help improve the manuscript.

Appendix A. Supplementary data

Supplementary data to this article can be found online at XXX.

References

Adya, D., Bayarkhuu, J., Dashtseren, Ts., Nymkhuu, T., 1970. Results of 1:200 000 scale geological mapping in the Adaatsag and Bayantsagaan regions. Ulaanbaatar, Geologic Information Center Open-File Report #1868 (in Russian).

Andersen, T. 2002. Correction of common lead in U-Pb analyses that do not report 204Pb, Chem. Geol. 192, 59–79.

Arzhannikova, A.V., Demonterova, E.I., Jolivet, M., Arzhannikov, S.G., Mikheeva, E.A., Ivanov, A.V., Khubanov, V.B., Pavlova, L.A., 2020. Late Mesozoic topographic evolution of western Transbaikalia: evidence for rapid geodynamic changes from the Mongol-Okhotsk collision to widespread rifting. Geosci. Front. 11, 1695–1709.

Arzhannikova, A.V., Demonterova, E.I., Jolivet, M., Mikheeva, E.A., Ivaanov, A.V., Arzhannikov, S.G., Khubanov, V.B., Kamenetsky, V.S., 2022. Segmental closure of the Mongol-Okhotsk Ocean: Insight from detrital geochronology in the East Transbaikalia Basin. Geosci. Front. 13, 101254

Badarch, G., Cunningham, W.D., Windley, B.F., 2002. A new block subdivision for Mongolia: implications for the Phanerozoic crustal growth of Central Asia. J. Asian Earth Sci. 21, 87–110.

Bussien, D., Gombojav, N., Winkler, W., Von Quadt, A., 2011. The Mongol-Okhotsk

Belt in Mongolia—a new appraisal of the geodynamic development by the study of sand-stone provenance and detrital zircons. Tectonophysics 510, 132–150.

Chen, L., Liang, C., Neubauer, F., Liu, Y., Zhang, Q., Song, Z., 2022. Sedimentary processes and deformation styles of the Mesozoic sedimentary succession in the northern margin of the Mohe basin, NE China: Constraints on the final closure of the Mongol–Okhotsk Ocean. J. Asian Earth Sci. 232, 105052.

Cogné, J.P., 2003. A Macintosh™ application for treating paleomagnetic data and making plate reconstructions. Geochem. Geophys. Geosyst. 4(1), 1007. https://doi.org/10.1029/2001GC000227

Cogné, J.-P., Kravchinsky, V.A., Halim, N., Hankard, F., 2005. Late Jurassic-Early Cretaceous closure of the Mongol-Okhotsk Ocean demonstrated by new Mesozoic palaeomagnetic results from the Trans-Baïkal area (SE Siberia). Geophys. J. Int. 163(2), 813-832.

Delvaux, D., Moeys, R., Stapel, G., Melnikov, A., Ermikov, V., 1995. Palaeostress reconstructions and geodynamics of the Baikal region, central Asia, Part I. Palaeozoic and Mesozoic pre-rift evolution. Tectonophysics 252, 61-101.

Demonterova, E. I., Ivanov, A. V., Mikheeva, E. M., Arzhannikova, A. V., Frolov, A. O., Arzannikov, S. G., 2017. Early to Middle Jurassic history of the southern Siberian continent (Transbaikalia) recorded in sediments of the Siberian Craton: Sm-Nd and U-Pb provenance study. Bull. Soc. Geol. France, 188(1–2), 8.

Donskaya, T.V., Gladkochub, D.P., Mazukabzov, A.M., Ivanov, A.V., 2013. Late Paleozoic – Mesozoic subduction-related magmatism at the southern margin of the Siberian continent and the 150 million-year history of the Mongol-Okhotsk Ocean. J. Asian Earth Sci. 62, 79–97.

Enkin, R. J., Yang, Z., Chen, Y., Courtillot, V., 1992. Paleomagnetic constraints on the geodynamic history of the major blocks of China from the Permian to the present. J. Geophys. Res. 97(B10), 13953-13989.

Fedorovskii, V.S., Dobrzhinetskaya, L.F., Molchanova, T.V., Likhachev, A.B., 1993. New type of melange: The Baikal Lake, Ol'khon region. Geotektonika 4, 30-45.

Fisher, R.,1953. Dispersion on a sphere, Proc. R. Soc. London, Ser. A, 217, 295–305.

Fu, W., Hou, H., Gao, R., Zhou, J., Zhang, X., Pan, Z., Huang, S., Guo, R., 2021. Lithospheric structures of the northern Hegenshan-Heihe suture: Implications for the Paleozoic metallogenic setting at the eastern segment of the central Asian orogenic belt. Ore Geol. Rev. 137, 104305.

Ganbat, A., Tsujimori, T., Miao, L., Safonova, I., Pastor-Galan, D., Anaad, C., Baatar, M., Aoki, S., Aoki, K., Savinskiy, I., 2021. Late Paleozoic–Early Mesozoic granitoids in the Khangay-Khentey basin, Central Mongolia: Implication for the tectonic evolution of the Mongol-Okhotsk Ocean margin. Lithos 404-405, 106455

Ge, W.C., Wu, F.Y., Zhou, C.Y., Abdel Rahman, A.A., 2005. Emplacement age of the Tahe granite and its constraints on the tectonic nature of the Erguna block in the northern part of the Da Xing'an Range. Chinese Sci. Bull. 50, 2097–2105 (in Chinese with English abstract).

Gladkochub, D., Pisarevsky, S., Donskaya, T., Natapov, L., Mazukabzov, A., Stanevich, A., Sklyarov, E., 2006. The Siberian Craton and its evolution in terms of the

Rodinia hypothesis. Episodes 29(3), 169-174.

Glebovitsky, V.A., Khil'tova, V.Ya., Kozakov, I.K., 2008. Tectonics of the Siberian Craton: Interpretation of Geological, Geophysical, Geochronological, and Isotopic Geochemical Data. Geotectonics 42, 8–20.

Gordienko, I.V., 1987. Paleozoic Magmatism and Geodynamics of Central Asian Foldbelt, Nauka, Moscow, p. 238.

Gordienko, I.V., 2006. Geodynamic evolution of Late Baikalides and Paleozoids in the folded periphery of the Siberian craton. Russian Geol. Geophys. 47, 53–70.

Gordienko, I.V., Metelkin, D.V., Vetluzhskikh, L.I., 2019. The Structure of the Mongol-Okhotsk Fold Belt and the Problem of Recognition of the Amur Microcontinent. Russian Geol. Geophys. 60, 267-286.

Gusev, G.S., and Khain, V.Y., 1996. On relations between the Baikal-Vitim, Aldan Stanovoy, and Mongol-Okhotsk blocks (south of mid-Siberia). Geotectonics 29(5), 422-436.

He, Z., Li, J., Mo, S., Sorokin, A. A., 2005. Geochemical discriminations of sandstones from the Mohe foreland basin, northeastern China: Tectonic setting and provenance. Sci. China Ser. D: Earth Sci. 48(5), 613-621.

Huang, B., Yan, Y., Piper, J.D.A., Zhang, D., Yi, Z., Yu, S., Zhou, T., 2018. Paleomagnetic constraints on the paleogeography of the East Asian blocks during Late Paleozoic and Early Mesozoic times. Earth-Sci. Rev. 186, 8–36.

Jolivet, M., De Boisgrollier, T., Petit, C., Fournier, M., Sankov, V. A., Ringenbach, J.C., Byzov, L., Miroshnichenko, A.I., Kovalenko, S.N., Anisimova, S.V., 2009. How old is the Baikal Rift Zone? Insight from apatite fission track thermochronology. Tectonics 28, TC3008. doi:10.1029/2008TC002404.

Jolivet, M., Arzhannikova, A., Frolov, A., Arzhannikov, S., Frolov, A., Arzhannikov, S., Kulagina, N., Akulova, V., Vassallo, R., 2017. Late Jurassic - Early Cretaceous paleoenvironmental evolution of the Transbaikal basins (SE Siberia): implications for the Mongol-Okhotsk orogeny. Bull. Soc. Géol. Fr., 188, 9.

Kalimulin, C.M., Durante, M.B., Zonenshain, L.P., Kalimulina, P.H., Filipova, I.B., Kozlovskii, Z.P., Pedorova, E.E., Pedorovoi., M.E., 1968. Results of 1:200 000 scale geological mapping in the Khentii region. Ulaanbaatar, Geologic Information Center Open-File Report #1758 (in Russian).

Kashiwagi, K., Tsukada, K., Minjin, C., 2004. Paleozoic spherical radiolarians from the Gorkhi Formation, southwest Khentei range, central Mongolia; a preliminary report. Mongolian Geoscientist 24, 17–26.

Kelty, T.K., Yin, A., Dash, B., Gehrels, G.E. and Ribeiro, A.E., 2008. Detrital-zircon geochronology of Paleozoic sedimentary rocks in the Hangay–Hentey basin, north-central Mongolia: implications for the tectonic evolution of the Mongol-Okhotsk Ocean in central Asia. Tectonophysics, 451, 290-311.

Khanchuk, A.I., Didenko, A.N., Popeko, L.I., Sorokin, A.A., Shevchenko, B.F., 2015. Structure and Evolution of the Mongol-Okhotsk Orogenic Belt, in Kröner, A., eds., The Central Asian Orogenic Belt. Geology, Evolution, Tectonics, and Models. Borntraeger Science Publishers, Stuttgart, Germany, 211–234.

Khosbayar, P., Bymbaa, B., Binderya, T., Gansukh, Z., Enkhtuvshin, Kh., Bataa, Ch.,

Erdenechimeg, J., Ganchimeg., Y., Adyasuren, L., Ganbat, B., 1987. Results of 1:200 000 scale geological mapping in the Ugiin Nuur region. Ulaanbaatar, Geologic Information Center Open-File Report #4135 (in Russian).

Kirschvink, J.L., 1980. The least-squares line and plane and the analysis of paleomagnetic data. Geophys. J. Royal Astron. Soc. 62(3), 699–718.

Kovalenko, V.I., Yarmolyuk, V.V., 1990. Evolution of magmatism in geological structures of Mongolia. In: Zaitsev, N.S., Kovalenko, V.I., (eds.). Evolution of Geological Processes. Nauka, Moscow, pp. 23-54. (in Russian)

Kravchinsky, V. A., Konstantinov, K.M., Cogne, J.P., 2001. Palaeomagnetic study of Vendian and Early Cambrian rocks of South Siberia and Central Mongolia: was the Siberian platform assembled at this time? Precambrian Res. 110, 61-92.

Kravchinsky, V.A., Sorokin, A.A., Courtillot, V., 2002. Paleomagnetism of Paleozoic and Mesozoic sediments from the southern margin of Mongol-Okhotsk ocean, far eastern Russia. J. Geophys. Res. 107 (B10), 2253.

Kurihara, T., Tsukada, K., Otoh, S., Kashiwagi, K., Chuluun, M., Byambadash, D., Boijir, B., Gonchigdorj, S., Nuramkhan, M., Niwa, M., Tokiwa, T., Hikchi, G., Kozuka, T., 2009. Upper Silurian and Devonian pelagic deep-water radiolarian chert from the Khangai–Khentei belt of Central Mongolia: Evidence for Middle Paleozoic subduction–accretion activity in the Central Asian Orogenic Belt. J. Asian Earth Sci. 34, 209–225.

Kuzmin, M.I., Kravchinsky, V.A., 1996. Preliminary paleomagnetic data on the Mongolia–Okhotsk fold belt. Russian Geol. Geophys. 37 (1), 54–62

Levashova, N.M., Van der Voo, R., Abrajevitch, A.V., Bazhenov, M.L., 2009. Paleomagnetism of mid-Paleozoic subduction-related volcanics from the Chingiz Range in NE Kazakhstan: the evolving paleogeography of the amalgamating Eurasian composite continent. Geol. Soc. Am. Bull. 121, 555–573.

Li, J., He, Z., Mo, S., Sorokin, A.A., 2004. The age of conglomerates in the lower part of the Xiufeng Formation in the northern Da Hinggan Mountains NE China, and their tectonic implications. Geol. Bull. China 23(2), 120-129.

Li, J., 2006. Permian geodynamic setting of Northeast China and adjacent regions: closure of the Paleo-Asian Ocean and subduction of the Paleo-Pacific Plate. J. Asian Earth Sci. 26, 207-224.

Ling, J., Li, P., Yuan, C., Sun, M., Zhang, Y., Narantsetseg, T., Wang, X., Jiang, Y., Hu, W., 2021. Ordovician to Devonian granitic plutons in the Hangay Range, Central Mongolia: Petrogenesis and insights into the Paleozoic tectonic evolution of the westernmost Mongol-Okhotsk Orogen. Lithos 404-405, 106463

Liu, Y., Li, W., Feng, Z., Wen, Q., Neubauer, F., Liang, C., 2017. A review of the Paleozoic tectonics in the eastern part of Central Asian Orogenic Belt. Gondwana Res. 43, 123-148.

Ludwig, K.R., 2003. User's Manual for Isoplot 3.0: A Geochronological, Toolkit for Microsoft Excel Berkeley Geochronology Center. special publication, vol. 4, pp. 1–71.

Ma, X. H., Xing, L. S., Yang, Z. Y., Xu, S. J., Zhang, J. X., 1993. Paleomagnetic study since Late Paleozoic in the Ordos Basin. Acta Geophys. Sinica, 36(1), 68–79. (in

Chinese with English Abstract).

Mao, A., Sun, D., Gou, J., Yang, D., Zhang, H., 2021. Late Palaeozoic–Early Mesozoic southward subduction of the Mongol–Okhotsk oceanic slab: geochronological, geochemical, and Hf isotopic evidence from intrusive rocks in the Erguna Massif (NE China). Int. Geol. Rev. 63, 1262-1287.

McFadden, P.L., & McElhinny, M.W. (1990) Classification of the reversal test in palaeomagnetism. Geophys. J. Int. 103, 725-729.

Metelkin, D.V., Vernikovsky, V.A., Kazansky, A. Yu., Wingate, M.T.D., 2010. Late Mesozoic tectonics of Central Asia based on paleomagnetic evidence. Gondwana Res. 18(2-3), 400-419.

Ovchinnikov, R.O., Sorokin, A.A., Xu, W.L., Kudryashov, N.M., 2023. Late Paleozoic and early Mesozoic granitoids in the northwestern Bureya Massif, Central Asian Orogenic Belt: Timing and tectonic significance. Int. Geol. Rev. https://doi.org/10.1080/00206814.2023.2178035

Parfenov, L.M., Popeko, L.I., Tomurtogoo, O., 1999. The problems of tectonics of the Mongol-Okhotsk orogenic belt. Pacific Oceanic Geol. 18(5), 24-43. (in Russian)

Paton, C., J. D. Woodhead, J. C. Hellstrom, J. M. He rgt, A. Greig, and R. Maas., 2010. Improved laser ablation U-Pb zircon geochronology through robust downhole fractionation correction. Geochem. Geophys. Geosyst. 11, Q0AA06

Pruner, P., 1992. Palaeomagnetism and palaeogeography of Mongolia from the Carboniferous to the Cretaceous—final report. Physics Earth Planet. Interiors 70, 169-177.

Rosen, O.M., Condie, K.C., Natapov, L.M., and Nozhkin, A.D., 1994. Archean and Early Proterozoic evolution of the Siberian craton: a preliminary assessment. in Condie, K.C., ed, Archean Crustal Evolution: Amsterdam, Elsevier, pp. 411–459.

Rosen, O.M., 2003. The Siberian craton: tectonic zonation and stages of evolution. Geotectonics 37, 175–192.

Ruppen, D., Knaf, A., Bussien, D., Winkler, W., Chimedtseren, A., Quadt, A., 2014. Restoring the Silurian to Carboniferous northern active continental margin of the Mongol–Okhotsk Ocean in Mongolia: Hangay–Hentey accretionary wedge and seamount collision. Gondwana Res. 25 (4), 1517–1534.

Sengör, A.M.C., Natal'in, B.A., Burtman, V.S., 1993. Evolution of the Altaid tectonic collage and Palaeozoic crustal growth in Eurasia. Nature 364, 299–307.

Seton, M., Müller, R.D., Zahirovic, S., Gaina, C., Torsvik, T., Shephard, G., Talsma, A., Gurnis, M., Turner, M., Maus, S., Chandler, M., 2012. Global continental and ocean basin reconstructions since 200 Ma. Earth-Sci. Rev.113, 212–270.

Sheldrick, T.C., Barry, T.L., Millar, I.L., Barfod, D.N., Halton, A.M., Smith, D.J., 2020. Evidence for southward subduction of the Mongol-Okhotsk oceanic plate: Implications from Mesozoic adakitic lavas from Mongolia. Gondwana Res. 79, 140-156.

Smirnova, Y. N., Sorokin, A., Popeko, L., Kotov, A., Kovach, V.P., 2017. Geochemistry and provenances of the Jurassic terrigenous rocks of the Upper Amur and Zeya–Dep troughs, eastern Central Asian fold belt. Geochem. Int. 55(2), 163–183.

Sorokin, A.A., Kotov, A.B., Kudryashov, N.M., Kovach, V.P., 2005. Late Paleozoic Urusha magmatic complex in the southern framing of the Mongolia-Okhotsk Belt (Amur Region): Age and geodynamic setting. Petrology 13, 596-610.

Sorokin, A.A., Kotov, A.B., Sal'nikova, E.B., Kudryashov, N.M., Anisimova, I.V., Yakovleva, S.Z., Fedoseenko, A.M., 2010. Granitoids of the Tyrma–Bureya complex in the northern Bureya–Jiamusi superterrane of the Central Asian fold belt: age and geodynamic setting. Russian Geol. Geophys. 51(5), 563-571.

Sorokin, A.A., Zaika, V.A., Kovach, V.P., Kotov, A.B., Xu, W., Yang, H., 2020. Timing of closure of the eastern Mongol–Okhotsk Ocean: Constraints from U–Pb and Hf isotopic data of detrital zircons from metasediments along the Dzhagdy Transect. Gondwana Res. 81, 58-78.

Sorokin, A.A., Zaika, V.A., Kadashnikova, A.Yu., Ponomarchuk, A.V., Travin, A.V., Ponomarchuk, V.A., Buchko, I.V., 2023. Mesozoic thermal events and related gold mineralization in the eastern Mongol-Okhotsk Orogenic Belt: constraints from regional geology and $^{40}Ar/^{39}Ar$ dating. Int. Geol. Rev. 65, 1476-1499.

Sun, D.Y., Gou, J., Wang, T.H., Ren, Y.S., Liu, Y.J., Guo, H.Y., Liu, X.M., Hu, Z.C., 2013. Geochronological and geochemical constraints on the Erguna massif basement, NE China–subduction history of the Mongol-Okhotsk oceanic crust. Int. Geol. Rev., 55, 1801-1816.

Tang, J., Xu, W., Wang, F., Wang, W., Xu, M., Zhang, Y., 2014. Geochronology and geochemistry of Early–Middle Triassic magmatism in the Erguna Massif, NE China: Constraints on the tectonic evolution of the Mongol–Okhotsk Ocean. Lithos 184-187, 1-16.

Tang, J., Xu, W., Wang, F., Zhao, S., Wang, W., 2016. Early Mesozoic southward subduction history of the Mongol–Okhotsk oceanic plate: Evidence from geochronology and geochemistry of Early Mesozoic intrusive rocks in the Erguna Massif, NE China. Gondwana Res. 31, 218–240.

Tomurtogoo, O., Windley, B.F., Kröner, A., Badarch, G., Liu, D.Y., 2005. Zircon age and occurrence of the Adaatsag ophiolite and Muron shear zone, central Mongolia: constraints on the evolution of the Mongol-Okhotsk ocean, suture and orogen. J. Geol. Soc. 162, 125-134.

Tomurtogoo O., 2014. Tectonics of Mongolia. In: Tectonics of Northern, Central and Eastern Asia, explanatory note to the Tectonic map of Northern Central Eastern Asia and adjacent areas at scale 1:2500000, p. 110–126.

Torsvik, T.H., Van der Voo, R., Preeden, U., Mac Niocaill, C., Steinberger, B., Doubrovine P.V., van Hinsbergen D.J.J., Domeier, M., Gaina, C., Tohver, E., Meert, J.G., McCausland, P.J.A., Cocks, R.M., 2012. Phanerozoic polar wander, palaeogeography and dynamics. Earth-Sciences Reviews 114, 325-368, doi:10.1016/j.earscirev.2012.06.007

Van der Voo, R., van Hinsbergen, D.J.J., Domeier, M., Spakman, W., Torsvik, T.H., 2015. Latest Jurassic–earliest Cretaceous closure of the Mongol-Okhotsk Ocean: A paleomagnetic and seismological-tomographic analysis, in Anderson, T.H., Didenko, A.N., Johnson, C.L., Khanchuk, A.I., and MacDonald, J.H., Jr., eds., Late Jurassic Margin of Laurasia-A Record of Faulting Accommodating Plate

Rotation. Geol. Soc. Am. Special Paper 513, 589–606.

Walderhaug, H.J., Eide, E.A., Scott, R.A., Inger, S., Golionko, E.G., 2005. Palaeomagnetism and 40Ar/ 39Ar geochronology from the south Taimyr igneous complex, Arctic Russia: A Middle-Late Triassic magmatic pulse after Siberian flood-basalt volcanism. Geophys. J. Int. 163(2), 501–517.

Wang, T., Tong, Y., Xiao, W., Guo, L., Windley, B.F., Donskaya, T., Li, S., Tserendash, N., Zhang, J., 2022. Rollback, scissor-like closure of the Mongol-Okhotsk Ocean and formation of an orocline: magmatic migration based on a large archive of age data. Natl. Sci. Rev. 9(5), nwab210.

Wang, W., Tang, J., Xu, W.-L., Wang, F., 2015. Geochronology and geochemistry of Early Jurassic volcanic rocks in the Erguna Massif, northeast China: Petrogenesis and implications for the tectonic evolution of the Mongol– Okhotsk suture belt. Lithos 218–219, 73–86.

Wu, L., Kravchinsky, V.A., Potter, D.K., 2017. Apparent polar wander paths of the major Chinese blocks since the Late Paleozoic: Toward restoring the amalgamation history of east Eurasia. Earth-Sci. Rev. 171, 492–519.

Xiao, W.J., Windley, B.F., Hao, J., Zhai, M.G., 2003. Accretion leading to collision and the Permian Solonker suture, Inner Mongolia, China: termination of the Central Asian Orogenic Belt. Tectonics 22, 1069.

Xu, B., Charvet, J., Chen, Y., Zhao, P., Shi, G., 2013a. Middle Paleozoic convergent orogenic belts in western Inner Mongolia (China): framework, kinematics, geochronology and implications for tectonic evolution of the Central Asian Orogenic Belt. Gondwana Res. 23, 1342-1364.

Xu, W.L., Pei, F.P., Wang, F., Meng, E., Ji, W.Q., Yang, D.B., Wang, W., 2013b. Spatial–temporal relationships of Mesozoic volcanic rocks in NE China: Constraints on tectonic overprinting and transformations between multiple tectonic regimes. J. Asian Earth Sci. 74, 167–193.

Yang, Y., Guo, Z., Song, C., Li, X., He, S., 2015. A short-lived but significant Mongol–Okhotsk collisional orogeny in latest Jurassic–earliest Cretaceous. Gondwana Res. 28, 1096–1116.

Yang, Z., Ma, X., Besse, J., Courtillot, V., Xing, L., Xu, S., Zhang, J., 1991. Paleomagnetic results from Triassic sections in the Ordos Basin, North China. Earth Planet. Sci. Lett. 104(2–4), 258–277.

Yi, Z., and Meert, J.G., 2020. A Closure of the Mongol-Okhotsk Ocean by the Middle Jurassic: Reconciliation of paleomagnetic and geological evidence. Geophys. Res. Lett. 47. e2020GL088235.

Zaika, V.A., Sorokin, A.A., Xu, B., Kotov, A.B., Kovach, V.P., 2018. Geochemical Features and Sources of Metasedimentary Rocks of the Western Part of the Tukuringra Block of the Mongol–Okhotsk Fold Belt. Stratigr. Geol. Correl. 26, 157–178.

Zhao, P., Chen, Y., Xu, B., Faure, M., Shi, G., Choulet, F., 2013. Did the Paleo-Asian Ocean between North China Block and Mongolia Block exist during the Late Paleozoic? First paleomagnetic evidence from central-eastern Inner Mongolia, China. J. Geophys. Res.: Solid Earth 118, 1873–1894.

Zhao, P., Xu, B., Jahn, B.M., 2017. The Mongol-Okhotsk Ocean subduction-related Permian peraluminous granites in northeastern Mongolia: Constraints from zircon U-Pb ages, whole-rock elemental and Sr-Nd-Hf isotopic compositions. J. Asian Earth Sci. 144, 225–242.

Zhao, P., Appel, E., Xu, B., Sukhbaatar, T., 2020. First paleomagnetic result from the Early Permian volcanic rocks in northeastern Mongolia: Evolutional implication for the Paleo-Asian Ocean and the Mongol-Okhotsk Ocean. J. Geophys. Res.: Solid Earth 125. https://doi.org/10.1029/2019JB017338

Zhao, P., Appel, E., Deng, C., Xu, B., 2023. Bending of the western Mongolian blocks initiated the Late Triassic closure of the Mongol-Okhotsk Ocean and formation of the Tuva-Mongol Orocline. Tectonics 42, e2022TC007475. https://doi.org/10.1029/2022TC007475

Zhao, X., Coe, R.S., Gilder, S.A., Frost, G.M., 1996. Palaeomagnetic constraints on the palaeogeography of China: implications for Gondwanaland. Aust. J. Earth Sci. 43, 643-672.

Zhao, X.X., Coe, R., Zhou, Y.X., et al., 1990. New paleomagnetic results from northern China, collision and suturing with Siberia and Kazakhstan. Tectonophysics 181, 43–81.

Zhou, J.B.,Wilde, S.A., Zhang, X.Z., Ren, S.M., Zheng, C.Q., 2011. Early Paleozoic metamorphic rocks of the Erguna block in the Great Xing'an Range, NE China: evidence for the timing of magmatic and metamorphic events and their tectonic implications. Tectonophysics 499, 105–117.

Zhou, J.B., Wang, B., Wilde, S.A., Zhao, G.C., Cao, J.L., Zheng, C.Q., Zeng, W.S., 2015. Geochemistry and U–Pb zircon dating of the Toudaoqiao blueschists in the Great Xing' an Range, northeast China, and tectonic implications. J. Asian Earth Sci. 97, 197–210.

Zhou, J.B., Wilde, S.A., Zhao, G.C., Han, J., 2018. Nature and assembly of microcontinental blocks within the Paleo-Asian Ocean. Earth-Sci. Rev. 186, 76–93.

Zhu, M., Zhang, F., Miao, L., Baatar, M., Anaad, C., Yang, S.H., Li, X.B., 2018. The late Carboniferous Khuhu davaa ophiolite in northeastern Mongolia: Implications for the tectonic evolution of the Mongol-Okhotsk ocean. Geol. J. 53, 1263-1278.

Zonenshain, L.P., Kuzmin, M.I., & Natapov, L.M., 1990. Geology of the USSR: plate tectonic synthesis. American Geophysical Union Geodynamics Series 21, 1-242.

Zorin, Y.A., Belichenko, V.G., Turutanov, E.K., Mazukabzov, A.M., Sklyarov, E.V., Mordvinova, V.V., 1995. The East Siberia Transect. Int. Geol. Rev. 37, 154–175.

Zorin, Y.A., 1999. Geodynamics of the western part of the Mongolia–Okhotsk collisional belt, Trans-Baikal region (Russia) and Mongolia. Tectonophysics 306, 33–56.

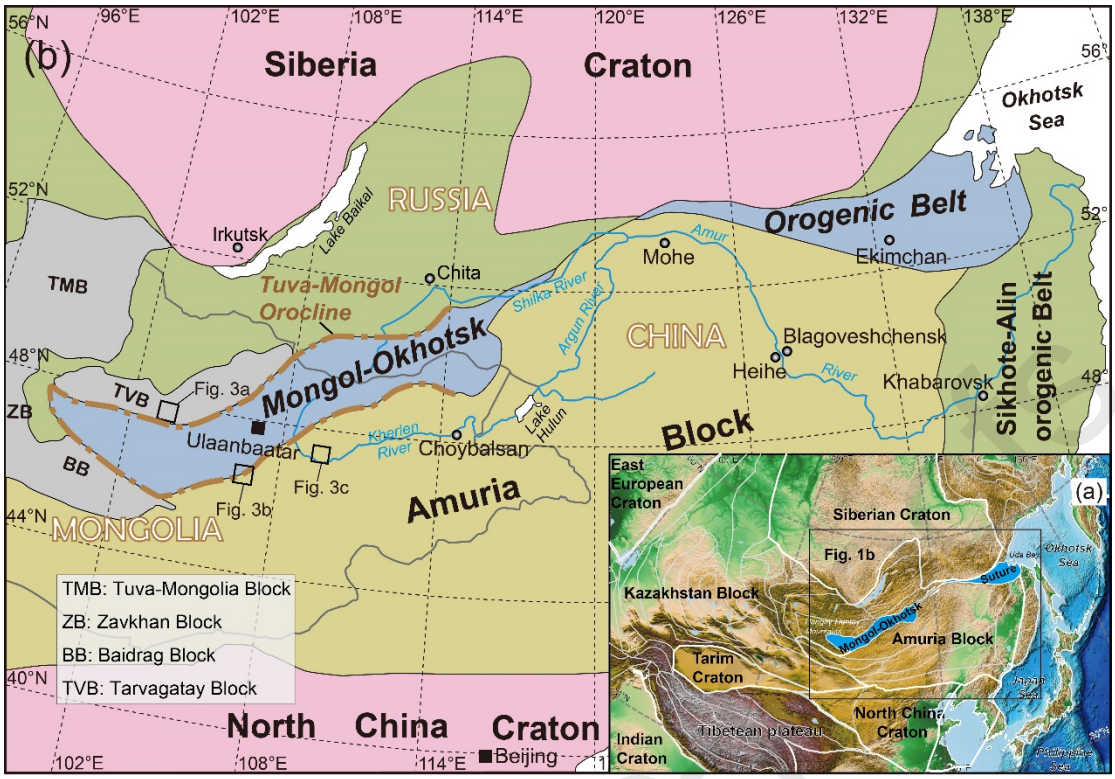

Figure 1. (a) Topography map of East Asia with major Precambrian blocks and location of the Mongol-Okhotsk suture. (b) Regional tectonic map showing the Siberia Craton, Amuria Block, central Mongolian blocks (including TMB: Tuva-Mongolia Block, ZB: Zavkhan Block, BB: Baidrag Block, and TVB: Tarvagatay Block), North China Craton, and the Mongol-Okhotsk orogenic belt extending from central Mongolia, through the Amur region to the Okhotsk Sea (modified from Zhao et al., 2020). Locations of three geological maps in figure 3 are marked.

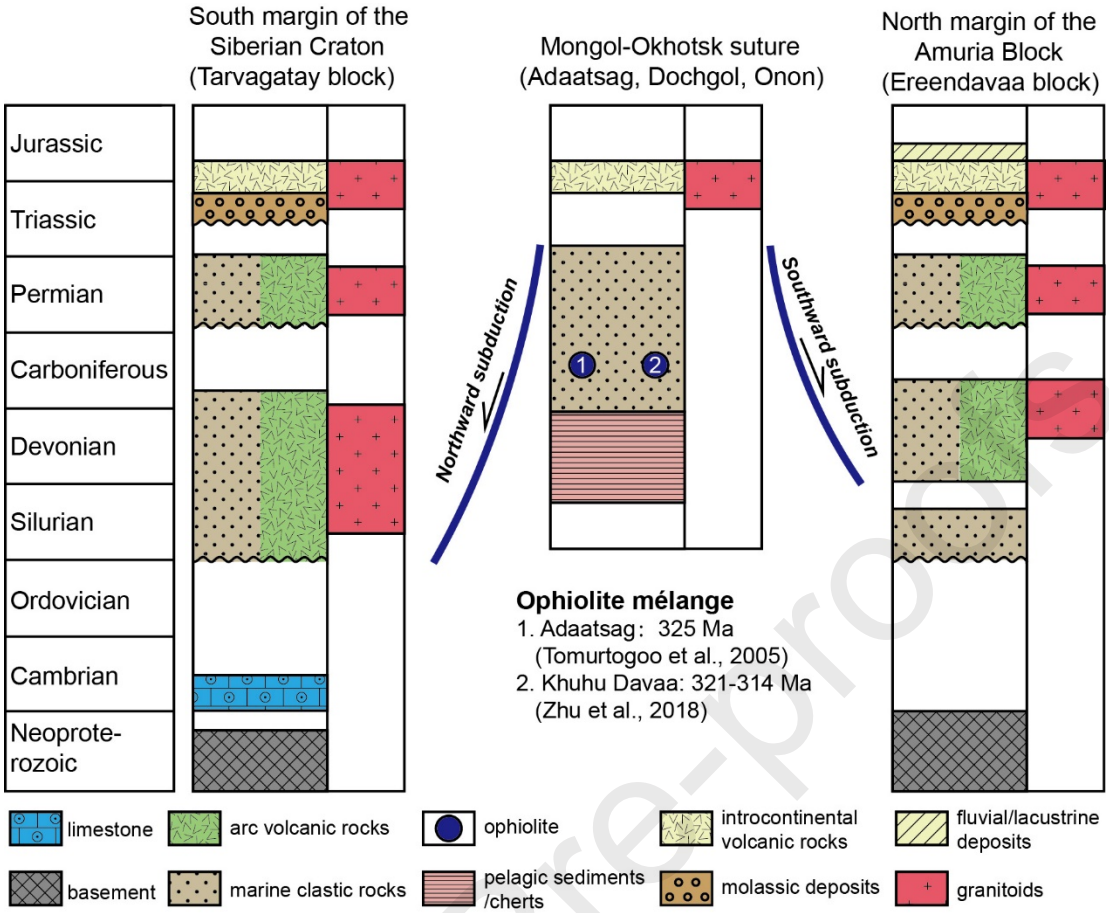

Figure 2. Tectonostratigraphic column of the Mongol-Okhotsk suture and Tarvagatay Block and northern Amuria Block on both sides of the suture (integrated from Zonenshain et al., 1990; Badarch et al., 2002; Bussien et al., 2011; Donskaya et al., 2013). Information of two ophiolite mélange are from Tomurtogoo et al. (2005) and Zhu et al. (2018).

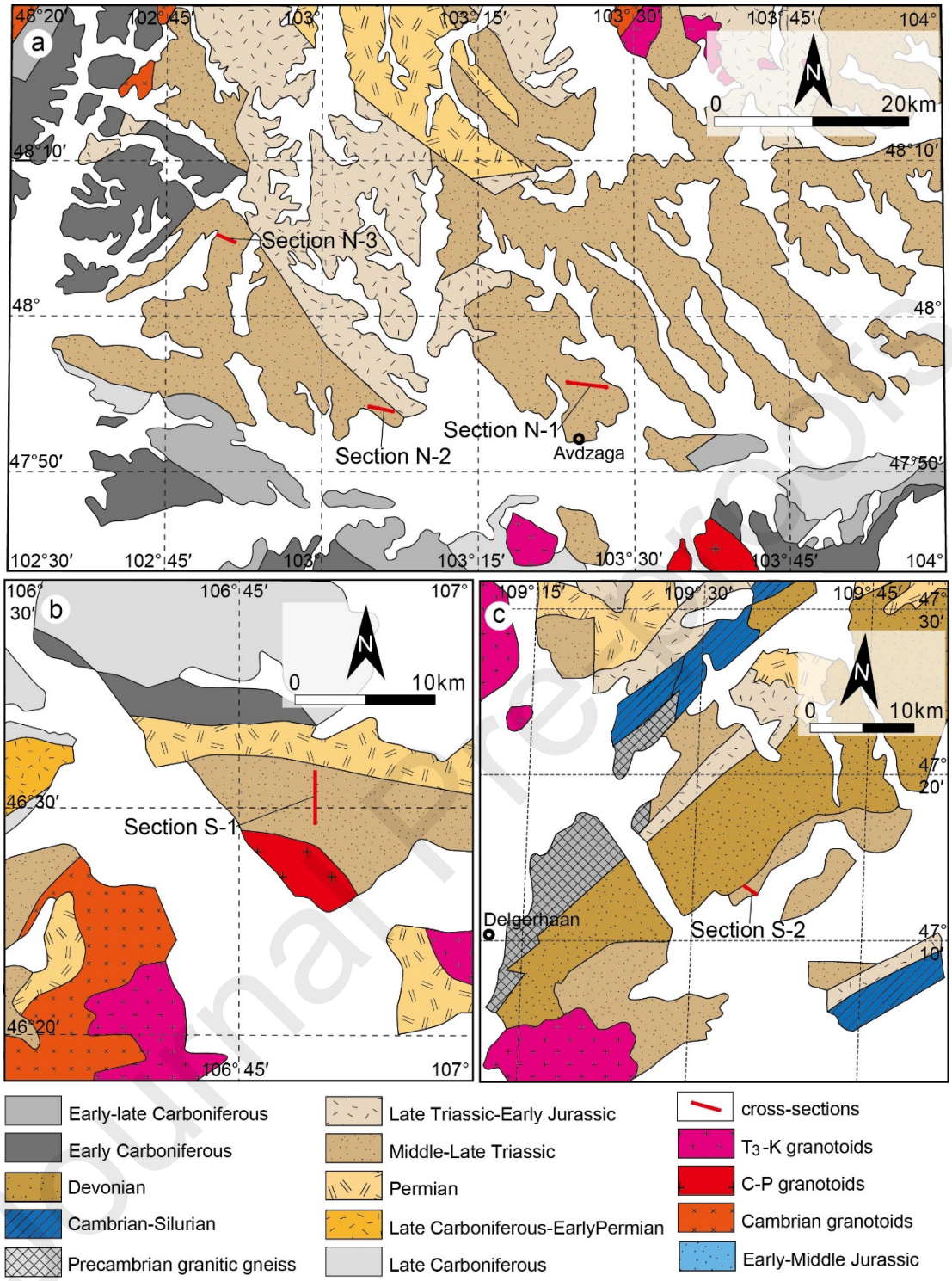

Figure 3. Geological map of the Avdzaga (a), Adaatsag (b) and Delgerhaan (c) regions showing locations of measured cross sections.

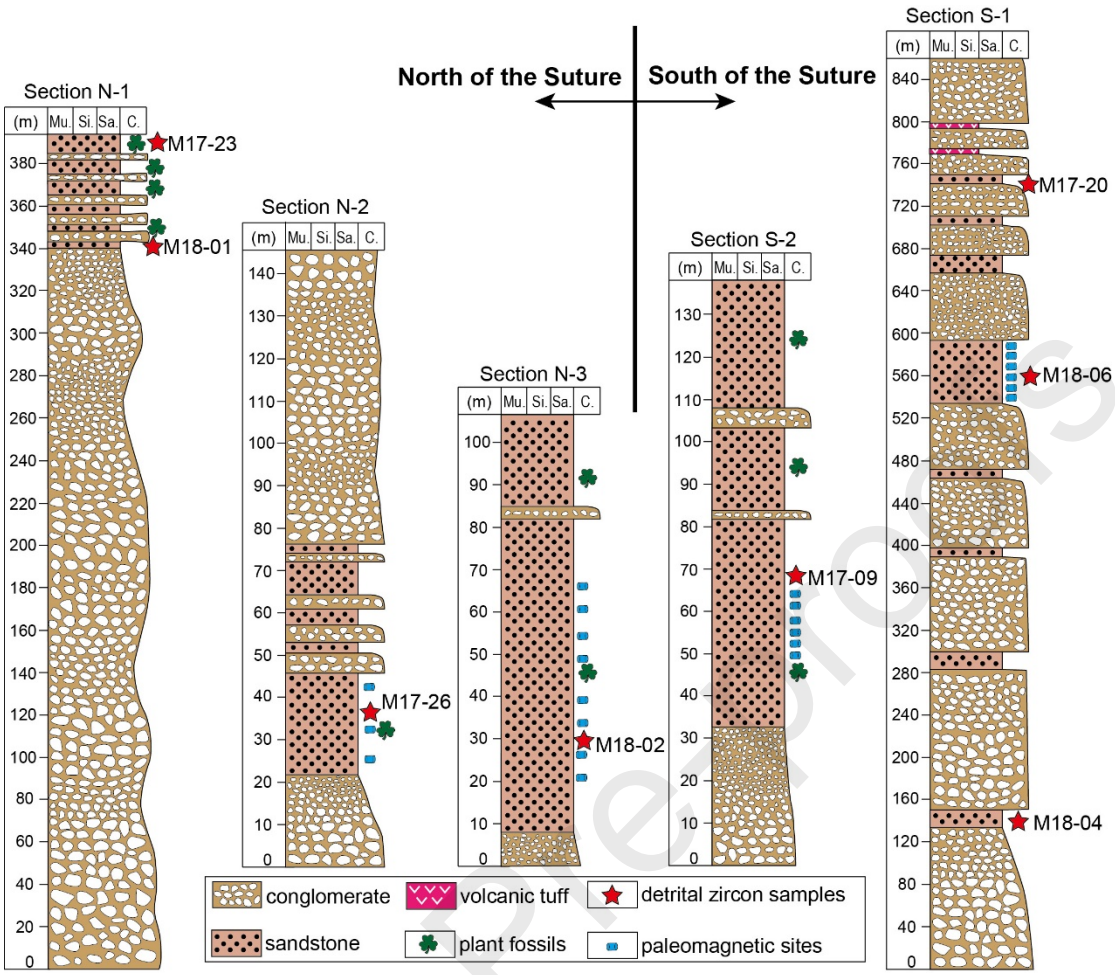

Figure 4. Stratigraphic columns of the five measured cross sections from both sides of the Mongol-Okhotsk suture with location of samples for detrital zircon U-Pb dating and paleomagnetic study. Mu., Mudstone; Si., Siltstone; Sa., Sandstone; C., Conglomerate.

Figure 5. Field outcrops of the upper Triassic strata from the Avdzaga region to the north of the Mongol-Okhotsk suture. (a and b) Basal conglomerate with pebbles of chert, granite, volcanic rocks and greeschist; (c and d) Interbedded conglomerate and sandstone; (e) Sandstone layers; (f) Cross bedding; (g) Parallel bedding; (h and i) Plant fossils.

Figure 6. Field outcrops of the upper Triassic strata from the Adaatsag and Delgerhaan regions to the south of the Mongol-Okhotsk suture. (a) Boulders from the basal conglomerate; (b) Basal conglomerate; (c) Cross bedding from coarse-grained sandstone layers; (d) Vertical red coarse-grained sandstone layers; (e and f) Plant fossils.

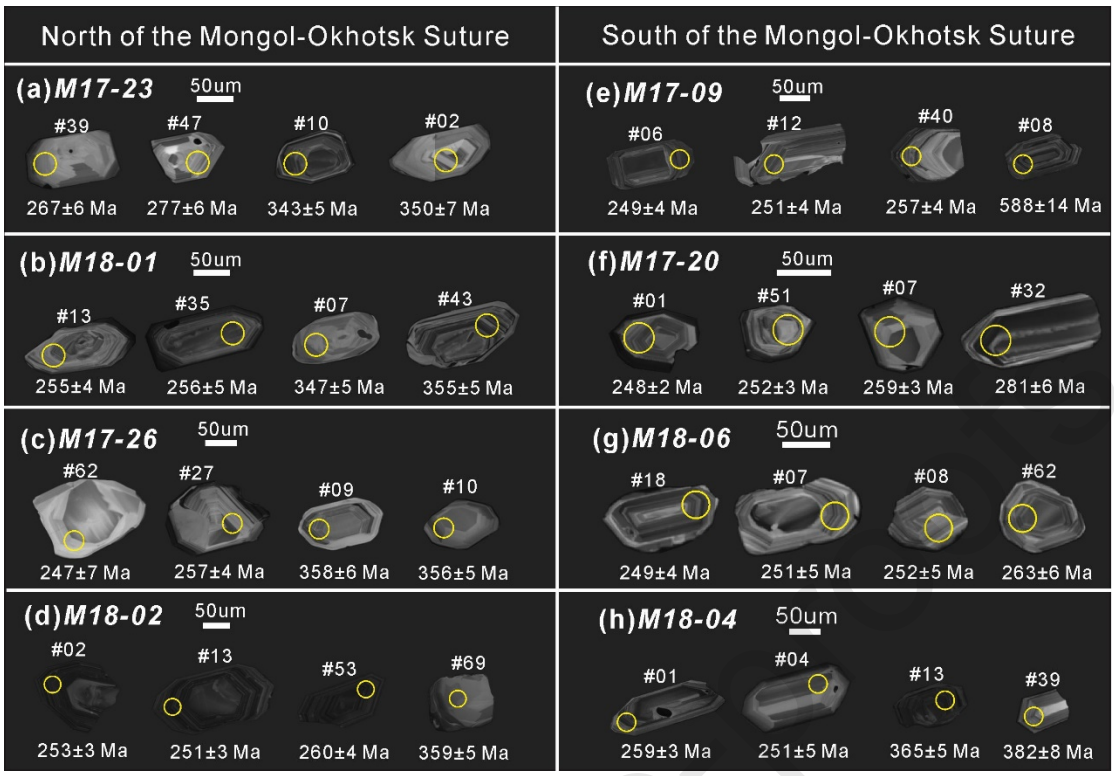

Figure 7. Cathodoluminescence (CL) images of selected detrital zircons from each sample. The yellow circles represent U–Pb analytical sites with numbers above and ages below the grain.

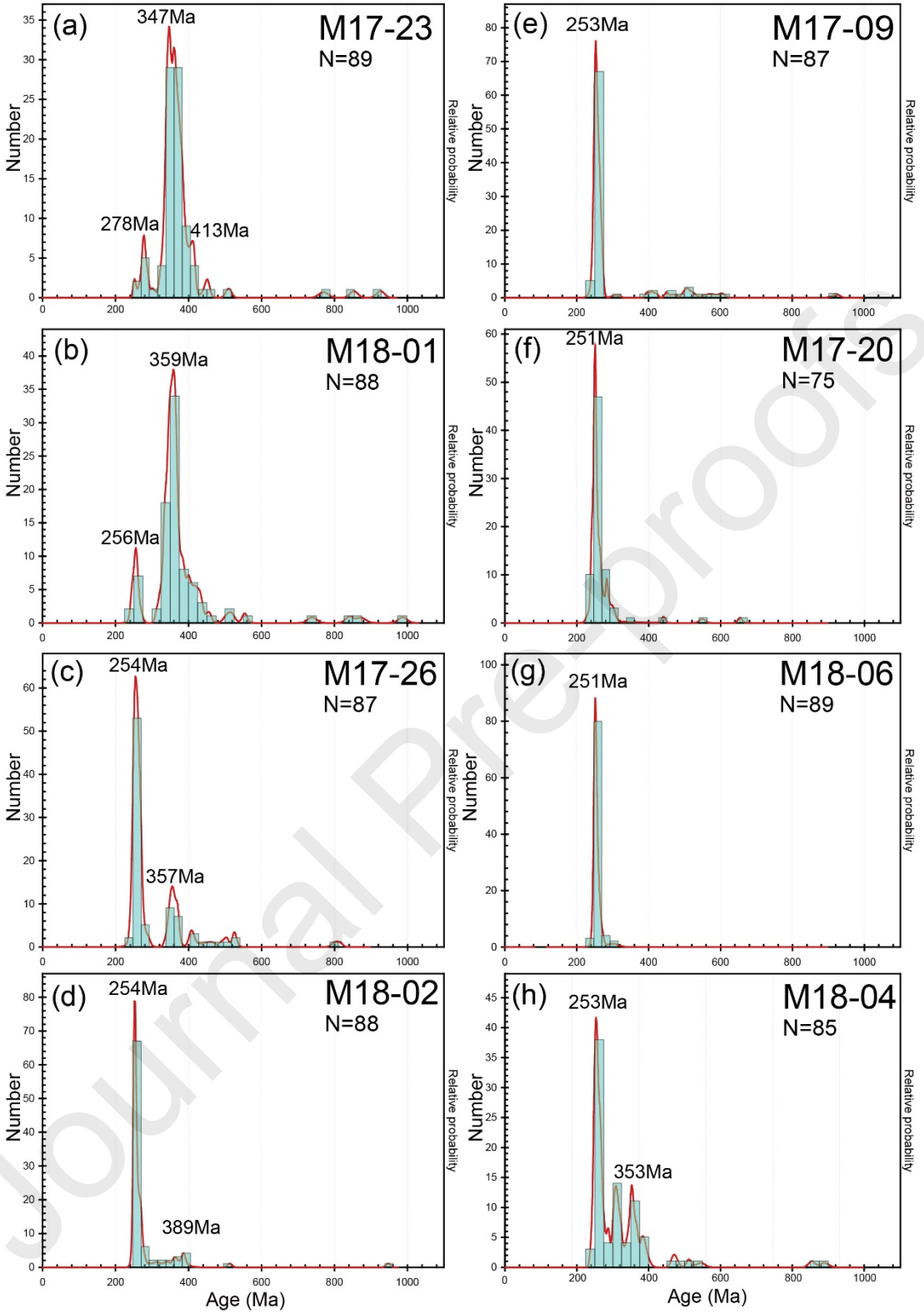

Figure 8. Probability diagrams of zircon ages of the eight sandstone samples in this study. Four samples (a-d) are from north of the Mongol-Okhotsk suture, and the other four samples (e-h) are from south of the Mongol-Okhotsk suture.

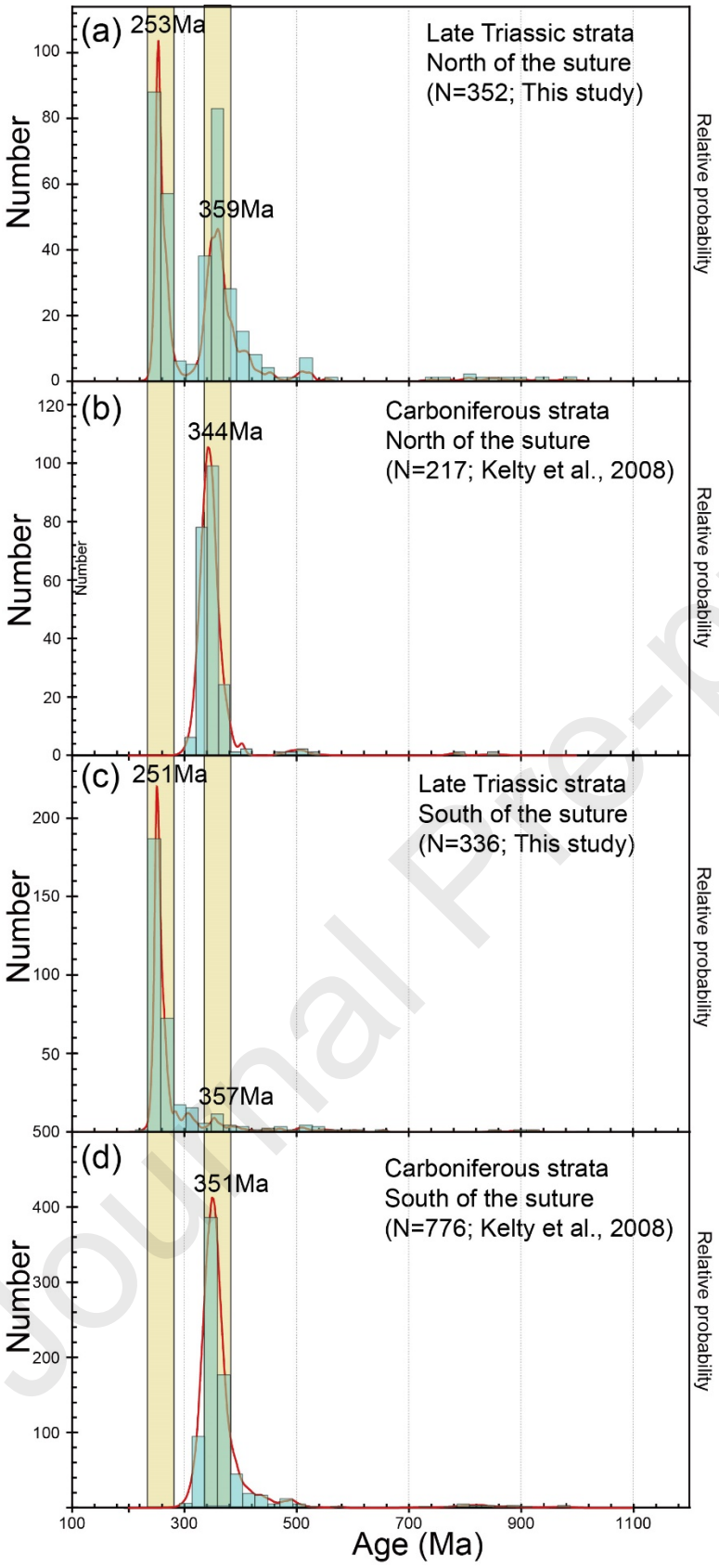

Figure 9. Comparison of probability plots for detrital zircon U-Pb ages from north (a and b) and south (c and d) sides of the Mongol-Okhotsk suture. Age data of the Carboniferous strata are from Kelty et al., 2008.

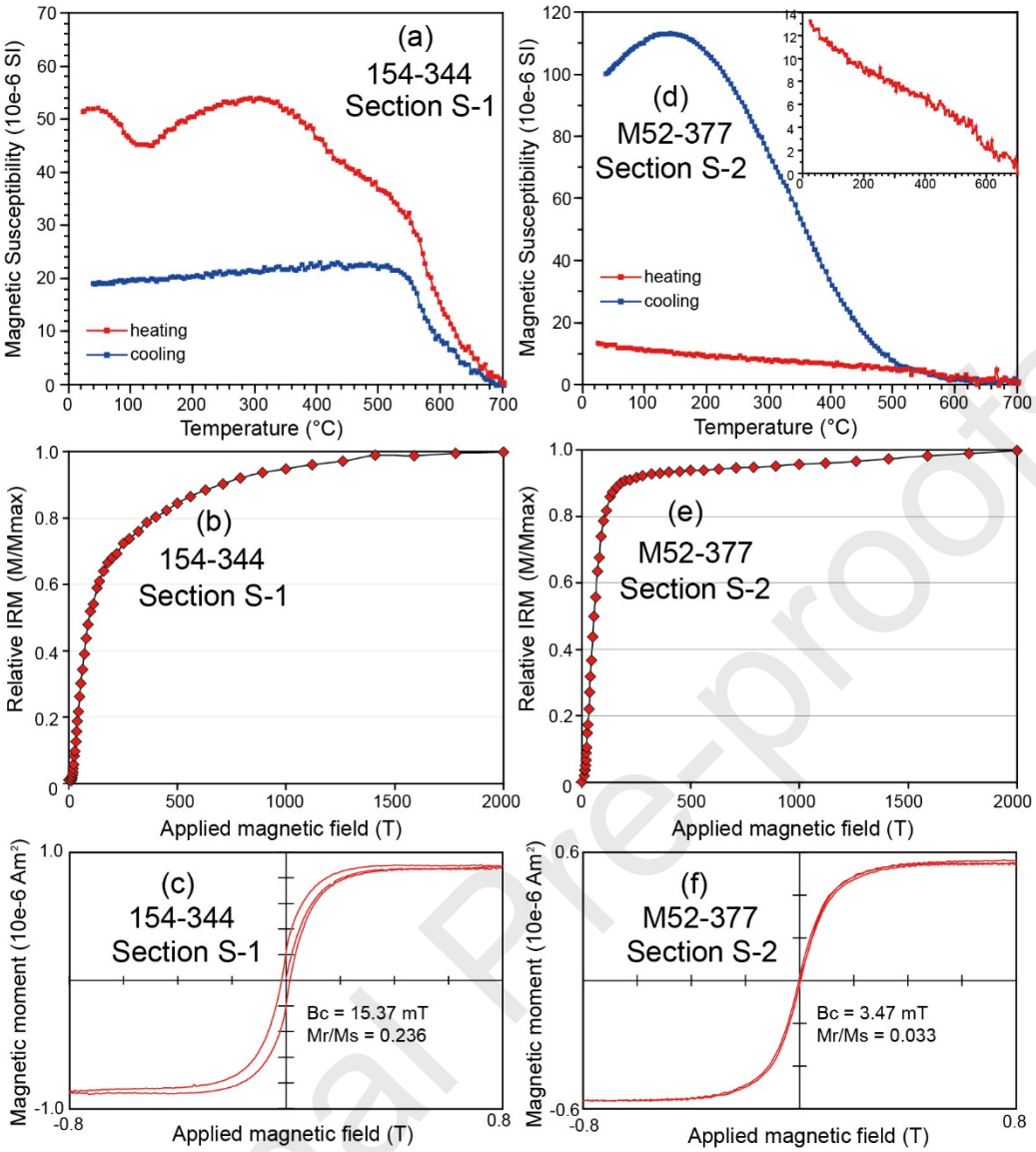

Figure 10. Magnetic mineral analyses for representative samples from Sections S-1 and S-2. Thermomagnetic curves (a and d; red/blue represent heating/cooling), isothermal magnetization acquisition curves (b and e), and magnetic hysteresis loops (c and f) of selected samples.

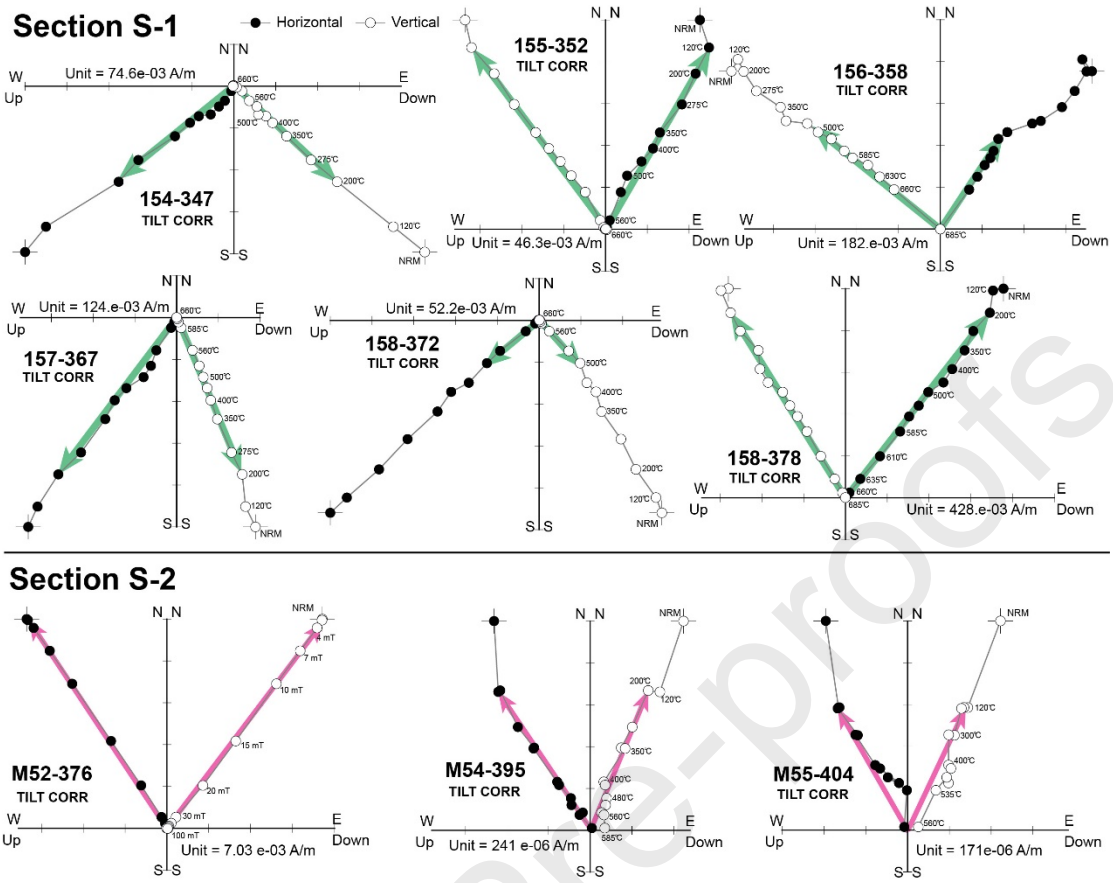

Figure 11. Representative orthogonal vector plots from sections S-1 and S-2. Directions are plotted in tilt-corrected coordinates. Black/white circles represent vector endpoints projected onto the horizontal/vertical plane. Numbers on the plots show temperature/applied alternating magnetic field steps. NRM: natural remanent magnetization.

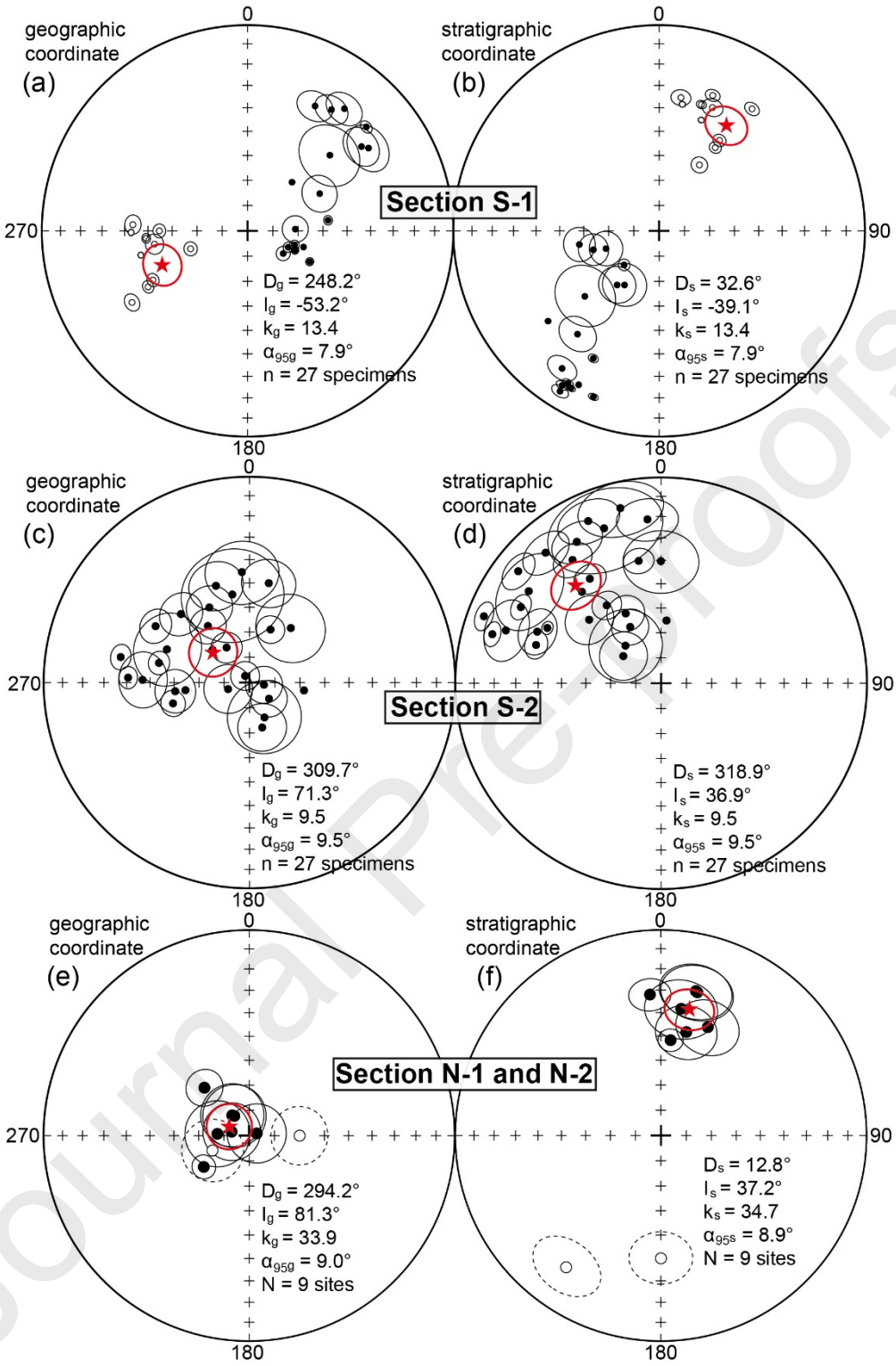

Figure 12. Equal-area projection of specimens from section S-1 (a and b) and S-2 (c and d) in geographic and stratigraphic coordinates. (e and f) Site-mean directions of nine sites from section N-1 and N-2 are presented for comparison (Zhao et al., 2023). Stars show overall specimen-/site-mean direction, solid circles represent normal polarity, while open circles represent reverse polarity.

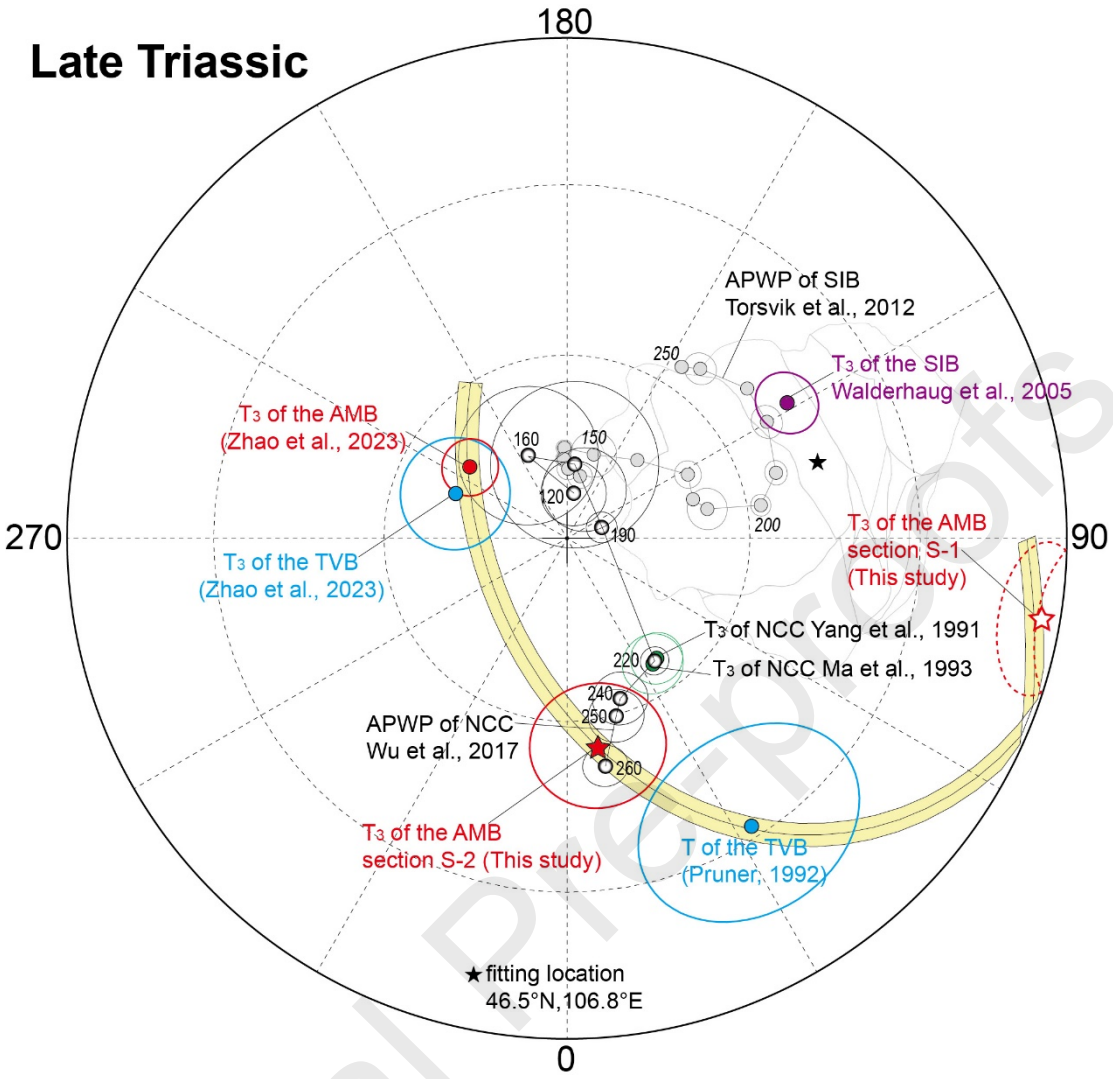

Figure 13. Comparison of the Late Triassic poles from the SIB, the TVB (Tarvagatay Block), AMB and NCC. Poles used in this figure are listed in Table 2. APWPs of both the NCC (Wu et al., 2017) and SIB (Torsvik et al., 2012) are plotted for comparison. The black star represents the fitting location. A small circle passes through the five Late Triassic poles of the AMB and the TVB, indicating consistent paleolatitude of the two blocks in the Late Triassic.

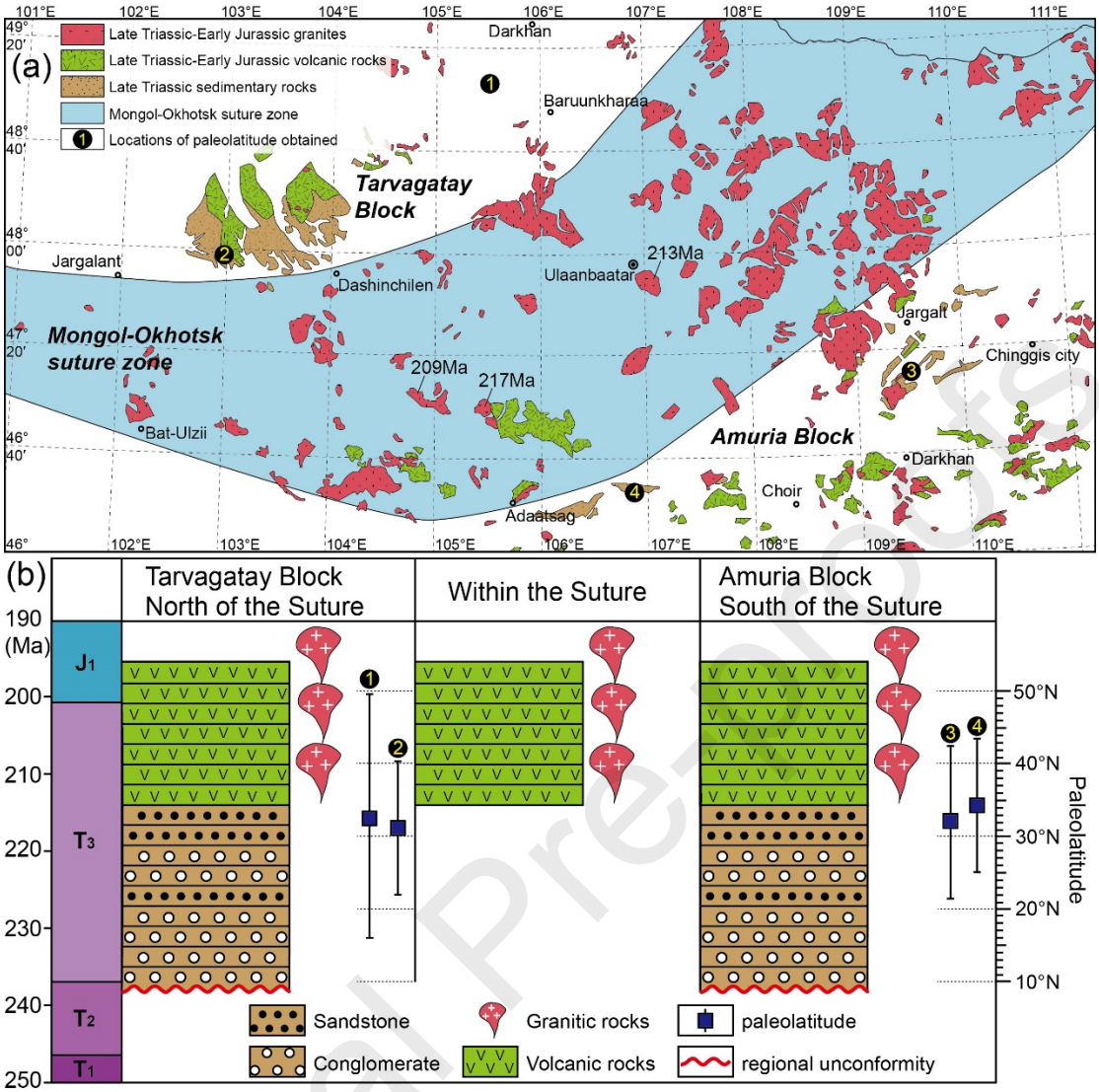

Figure 14. (a) Geological map of the western segment of the Mongol-Okhotsk suture with emphasis on the Late Triassic-Early Jurassic sedimentary and volcanic sequence within and around the suture, and highlight the Late Triassic stitching plutons that intruded the suture (from Wang et al., 2022). Numbers of 1-4 represent locations where the Late Triassic paleolatitude data obtained from both sides of the sure. (#1 from Pruner, 1992; #2 from Zhao et al., 2023; #3 and 4 from this study). (b) Integrated columns of the Mongol-Okhotsk Suture, and Tarvagatay Block and Amuria Block on both sides of the suture with consistent Late Triassic sedimentary sequence, magmatic rocks and paleolatitude, indicating that the Mongol-Okhotsk Ocean should have closed in its western segment at least by the Late Triassic.

Table 1. Paleomagnetic sampling information and results (HTC component) of the Late Triassic sandstone from both sides of the Mongol-Okhotsk suture zone.

Site	coordinate	rock type	dip dir./angle	n'/n	N/R	Dg	Ig	Ds	Is	k	α_{95}	Ds*	Is*	k*	α_{95}*	comment
Sandstone from Adaatsag region (section S-1), Amuria Block																
154	46°29'18"N,106°51'09"E	red sandstone	228/85	8/8	8/0	45.3	34.6	232.5	60.3	31.3	10.1					
155	46°29'19"N,106°51'08"E	red sandstone	228/85	4/8	0/4	269.6	-47.6	15.1	-34.5	185.3	6.8					
156	46°29'20"N,106°51'08"E	red sandstone	228/85	4/7	0/4	244.3	-43.0	29.6	-49.3	90.7	9.7					
157	46°29'20"N,106°51'07"E	red sandstone	228/85	7/7	7/0	109.3	69.8	209.8	14.3	237.8	3.9					
158	46°29'21"N,106°51'06"E	red sandstone	228/85	4/7	2/2	71.6	61.0	214.8	31.3	54.1	12.6					
159	46°29'21"N,106°51'06"E	red sandstone	228/85	6/7	6/0	156.0	30.4	170.7	-12.8	193.1	4.8					
	Mean (5 sites) exclude site 159					25	-			16.	1					

						0.8	53.0			6	9.3						
								30.6	-38.5	16.6	19.3						
Mean (27 specimens) exclude site 159						248.2	-53.2			13.4	7.9						
								32.6	-39.1	13.4	7.9	32.6	-53.7	13.4	7.9		
VGP (27 specimens)						***λ=-4.1°, φ=80.3°, A_{95}=9.2°, Paleolat.=34.2°***											
Yellow sandstone from Delgerhaan region (section S-2), Amuria Block																	
M52	47°11'58"N,119°32'36"E	sandstone	325/35	6/7	0/0	-	-	-	-	-	-	-	-	-	-	dispersed	
M53	47°11'56"N,119°32'38"E	sandstone	325/35	5/7	5/0	289.7	53.3	297.4	18.6	21.6	16.9	-	-	-	-	dispersed	
M54	47°11'59"N,119°32'38"E	sandstone	325/35	0/7	0/0	-	-	-	-	-	-	-	-	-	-	dispersed	
M55	47°12'01"N,119°32'41"E	sandstone	325/35	5/7	5/0	358.5	75.5	329.2	38.4	12.2	22.8	-	-	-	-	dispersed	
M5	47°12'01"N,119°	sandstone	325/	7/	6/	29	72.	31	39.	12.	1	-	-	-	-	dispers	

6	32'41"E		35	7	0	7.8	8	5.0	1	5	9.7					ed
M57	47°12'02"N,119°32'40"E	sandstone	325/35	5/7	5/0	-	-	-	-	-	-	-	-	-	-	dispersed
	Mean (27 specimens)					309.7	71.3			9.5	9.5					
								318.9	36.9	9.5	9.5	318.9	51.4	9.5	9.5	
	VGP (27 specimens)										***λ=55.4°, φ=18.6°, A_{95}=10.6°, Paleolat.=32.1°***					
Sandstone from Avdzaga region (sections N-1 and N-2), Mongolia, Tarvagatay terrane (published in Zhao et al., 2023)																
114	47°53'54"N,103°06'22"E	sandstone	20/46	6/7	6/0	74.0	86.9	23.4	42.1	33.5	11.7	23.5	48.0	34.7	11.5	
115	47°53'54"N,103°06'21"E	sandstone	24/44	4/7	3/1	282.5	82.9	13.8	47.0	66.1	11.4	13.9	53.2	82.1	10.2	
116	47°53'54"N,103°06'21"E	sandstone	24/44	5/7	5/0	316.9	63.9	355.5	31.8	110.6	7.3	355.5	37.8	121.0	7.0	
124	48°05'24"N,102°49'03"E	sandstone	144/56	5/8	5/0	82.9	80.3	134.3	28.9	38.7	12.5	14.2	34.4	38.1	12.6	
125	48°05'25"N,102°49'04"E	sandstone	144/56	8/8	8/0	355.4	68.1	125.8	51.5	138.9	4.7	5.8	57.4	162.3	4.4	
12	48°05'25"N,102°	sandstone	144/	5/	0/	7.9	-	33	-	39.	1	215.5	-	40.	12.	

6	49'04"E		56	7	5		74.3	5.7	22.1	6	2.3		26.9	6	2
127	48°05'26"N,102°49'06"E	sandstone	144/56	6/8	6/0	33.2	77.4	129.1	37.6	27.6	13.0	8.8	43.4	29.2	12.6
128-129	48°05'26"N,102°49'06"E	sandstone	144/56	8/14	7/1	80.3	79.5	133.6	28.5	20.6	12.5	13.5	33.4	20.5	12.5
130	48°05'24"N,102°49'04"E	sandstone	144/56	7/7	-	-	-	-	-	-	-				
131	48°05'24"N,102°49'06"E	sandstone	144/56	7/7	0/7	210.1	-70.0	300.0	-39.9	29.1	11.4	179.9	-45.8	32.3	10.8
	Mean (9 sites)					294.2	81.3			33.9	9.0				
								12.8	37.2	34.7	8.9	12.9	50.3	40.0	8.2
	VGP (9 sites)							***λ=70.5°, φ=248.2°, A_{95}=9.0°, Paleolat.=31.1°***							

Abbreviations. n'/n: numbers of accepted/measured samples; N/R: normal/reverse polarity; Dg, Ig, Ds, Is: declination (D) and inclination (I) in geographic (g) and tilt-corrected (s) coordinates; k: precision parameter; α_{95}: 95% confidence. *: values after E/I correction with inclination shallow factor f=0.6 following Van der Voo et al., 2015 and Wu et al., 2017 for better comparison.

For red sandstone from the Adaatsag region: both normal and reversed polarities existed. When use 5 site-mean directions, reversal test of McFadden and McElhinny (1990) is indeterminate; however, when we use 27 specimen directions for calculation, reversal test of McFadden and McElhinny (1990) is positive at level-C as the angle between the mean directions of normal (D/I = 256.7°/-48.7°, k = 42.8, n = 10) and reversed (D/I = 61.8°/55.6°, k = 9.9, n = 17) specimens γ=11.5° < $\gamma_{critical}$ = 16.0°.

For sandstone from the Avdzaga region: site-mean directions of sites 124-131 were rotated 120° counterclockwise and then calculate formation-mean direction with sites 114-116. Fold tests are indeterminate. The reversal test of McFadden and McElhinny (1990) is positive at level-B as the angle between the mean directions of normal (D/I = 10.3°/38.7°, k = 27.4, n = 40) and reversed (D/I = 197.2°/-34.3°, k = 12.9, n = 14) specimens

γ=7.1° < $\gamma_{critical}$ = 9.9°.

Table 2. Compilation of Late Triassic paleomagnetic poles from the North China Craton, Amuria Block, Tarvagatay Block and Siberian Craton. Abbreviations: N, number of locations (L), sites (S), or samples (s) used for calculation; Slat (Plat), latitude of sampling site (pole); Slong (Plong), longitude of sampling site (pole); A_{95}, 95% confidence limit; F, fold test; R, reversal test.

Age	Slat (°N)	Slong (°E)	N	Plat (°N)	Plong (°E)	A_{95}(°) (dp/dm)	Test	Paleolatitude (°N)	References
North China Craton (NCC)									
T_3*	35.2	109.1	19S	65.2	34.4	5.6	R	37.8±5.6	Ma et al., 1993
T_3*	35.2	109.2	11S	65.6	36.1	4.7	F+R	38.5±4.7	Yang et al., 1991
Amuria Block (AMB)									
Inner Mongolia (China)									
T_3*	43.7	118.8	15S	70.4	233.8	4.6	F+R	33.3±4.6	Zhao et al., 2023
Mongolia									
T_3*	46.5	106.9	27s	-4.1	80.3	9.2	R	34.2±9.2	This study
T_3*	47.4	109.5	27s	55.4	18.6	10.6	-	32.1±10.6	This study
Tarvagatay Block									
T_3*	47.9	103.1	9S	70.5	248.2	9.0	-	31.1±9.0	Zhao et al., 2023
T_3	49.1	105.5	6S	32.2	32.7	16.8	R	32.8±16.8	Pruner, 1992
Siberian Craton (SIB)									
T_3(228Ma)	74.8	100.6	13S	47.1	121.6	4.8/5.3	F	60.9±5.0	Walderhaug et al., 2005

*Triassic poles obtained from sedimentary rocks (mainly red sandstone/siltstone). Both poles and paleolatitudes were recalculated after inclination shallowing correction with inclination shallowing factor $f = 0.6$.

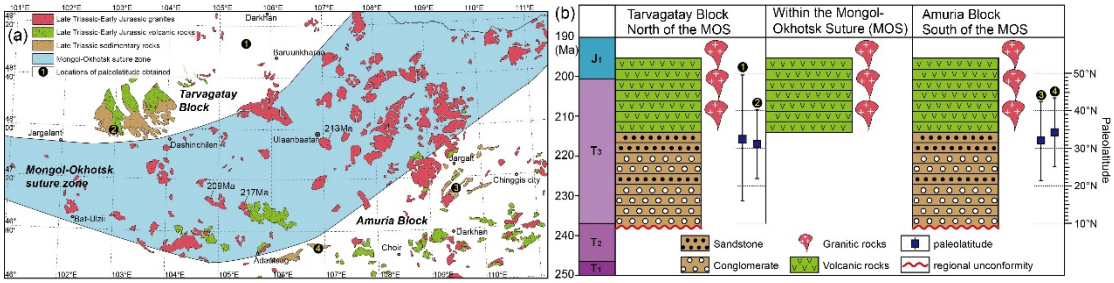

Highlights:

- Similar Late Triassic nonmarine strata were identified on both sides of the suture.
- Consistent paleolatitude of the Amuria Block and Tarvagatay Block in Late Triassic.
- Initial closure of the Mongol-Okhotsk Ocean occurred in the Late Triassic.

The authors declare that they have no known competing financial interests or personal relationships that could have appeared to influence the work reported in this paper.

CRediT authorship contribution statement

Pan Zhao: Conceptualization, Methodology, Formal analysis, Data curation, Writing–original draft, Writing–review & editing, Visualization. **Zhenhua Jia:** Methodology, Formal analysis, Writing–review & editing. **Bei Xu:** Data curation, Writing–review & editing. **Yan Xu:** Methodology, Data curation, Writing–review & editing. **Turbold Sukhbaatar:** Writing–review & editing. **Erwin Appel:** Methodology, Data curation, Writing–review & editing. **Yan Chen:** Methodology, Data curation, Writing–review & editing.